Uncertainty of low-degree space gravimetry observations: surface processes versus internal signal

Hugo Lecomte[1], Séverine Rosat[1], Mioara Mandea[2], Jean-Paul Boy[1], Julia Pfeffer[3]

[1]Université de Strasbourg, CNRS, EOST, ITES UMR7063, F-67000 Strasbourg, France
[2]Centre National d'Etudes Spatiales, Paris, France
[3]Magellium, Ramonville Saint-Agne, France

Key Points:

- Deep Earth's processes occur at large spatial and inter-annual temporal scales
- Time-lapse gravity satellite data are compared with geophysical models at scales of interest
- Large uncertainties on satellite data and geophysical models conceal the gravity signals originated from the Earth's core

Corresponding author: Hugo Lecomte, `hlecomte@unistra.fr`

Abstract

Space gravity measurements have been mainly used to study the temporal mass variations at the Earth's surface and within the mantle. Nevertheless, mass variations due to the Earth's core might be observable in the variations of the gravity field as measured by GRACE(-FO) satellites. Earth's core dynamical processes inferred from geomagnetic field measurements are characterized by large-scale patterns associated with low spherical harmonic degrees of the potential fields. To study these processes, the use of large spatial and inter-annual temporal filters is needed. To access gravity variations related to the Earth's core, surface effects must be corrected, including hydrological, oceanic or atmospheric loading (Newtonian attraction and mass redistribution associated with elastic deformation). However, these corrections for surface processes add errors to the estimates of the residual gravity field variations enclosing deep Earth's signals. As our goal is to evaluate the possibility to detect signals of core origin embedded in the residual gravity field variations, a quantification of the uncertainty associated with gravity field products and geophysical models used to minimise the surface process signatures is necessary. Here, we estimate the dispersion for GRACE solutions as about 0.34 cm of Equivalent Water Height (EWH) or 20% of the total signal. Uncertainty for hydrological models is as large as 0.89 to 2.10 cm of EWH. We provide estimates of some Earth's core signals which amplitudes are compared with GRACE gravity field residuals and uncertainties. The results presented here underline how challenging is to get new information about the dynamics of the Earth's core via high-resolution, high-accuracy gravity data.

Plain Language Summary

The motions of the Earth's fluid core are deduced from ground and satellite measurements of the geomagnetic field variations. Because the long-term variations of the Earth's gravity field might be correlated to the Earth's magnetic field, new information about the Earth's fluid core and its density changes could be accessed with gravimetry. The observation of the core processes must be done at very large spatial scales, in which case it is necessary to use gravity data from satellites. However, variations in the Earth's gravity field are also created by heterogeneous superficial sources such as ocean and atmospheric currents, variations in water storage, etc. To recover a signature of the Earth's fluid core, we need first to remove all other known effects of larger amplitudes from satellite observations of the gravity field. Our study compares models of gravity variations for different sources

in order to estimate their uncertainty. Such uncertainties are discussed in view of the expected amplitudes of signals originated from the core.

1 Introduction

Gravity field variations measured by the Gravity Recovery and Climate Experiment (GRACE) and GRACE Follow-On (GRACE-FO) missions are sensitive to the redistribution of masses located above, at or below the Earth's surface (Chen et al., 2022). GRACE & GRACE-FO (referred to as GRACE) satellite data are used to estimate the Earth's mass variations from regional to global scales since 2002 (Tapley et al., 2004; Landerer et al., 2020). For example, GRACE satellite data became essential to monitor the evolution of terrestrial water storage, ice sheets, glaciers and sea level in a worldwide changing climate (Tapley et al., 2019). GRACE satellite data are, by nature, integrative, so that it may be difficult to separate the sources of change in the gravity field. Each process has a specific spatial and temporal signature that can go from global to local and from the secular to the sub-daily scales (Fig. 1). We refer to certain surface processes with the term "loading" defined here as the Newtonian attraction and mass redistribution associated with elastic deformation. By approximate order of magnitude, the processes include in GRACE records are tidal effects from extraterrestrial bodies, post-glacial rebound (Purcell et al., 2011), hydrological (Rodell et al., 2018), atmospheric (Kusche & Schrama, 2005) and oceanic (Dobslaw et al., 2017) loading, water mass displacement across ocean, hydrosphere and cryosphere (Pfeffer et al., 2021), pre-seismic (Bouih et al., 2022), co-seismic and post seismic (Deggim et al., 2021) mass re-distributions, sea level changes (Adhikari et al., 2019; Horwath et al., 2022) and finally core processes.

In addition to its primary purposes, some new applications of the GRACE measurements were proposed to study the deep Earth's interior. Panet et al. (2018) gave an example of possible seismic precursor in the mantle before Tohoku earthquake in 2011; this kind of signature was also observed before the Maule-Chile event (Bouih et al., 2022). Other authors have proposed to improve the knowledge of the dynamical processes of the Earth's core. Dumberry (2010a); Dumberry and Mandea (2021) predicted a gravity perturbation generated by various core processes that might be observable on the low degrees of the gravity field. No signature of these perturbations has yet been observed in the gravity variations. However, Mandea et al. (2012) showed a correlation between the variations of the geomagnetic field and the gravity field. Processes of dissolution and crystallization at the core-mantle boundary (CMB) were advocated to explain this correlation (Mandea et al., 2015).

Established methods of seismic tomography, Earth's rotation, gravity and geomagnetic data analysis and geodynamic modelling constrain distributions of seismic velocity, density, electrical conductivity, and viscosity at depth, all depending on the internal structure of the Earth. Global Earth's interior models based on different observables often lead to rather different images. For example, the analysis of the time-variable magnetic field allows to focus on the dynamical features of the core field (Gillet et al., 2010, 2022). On the other hand, gaining information about the Earth's core from the analysis of the gravity field is difficult, because it requires to separate the different sources of signal with independent observations and/or models. In this context, gravimetry has the potential to bring new constraint about the density anomalies in the core and at its boundaries in a complimentary way to seismology (Koelemeijer, 2021).

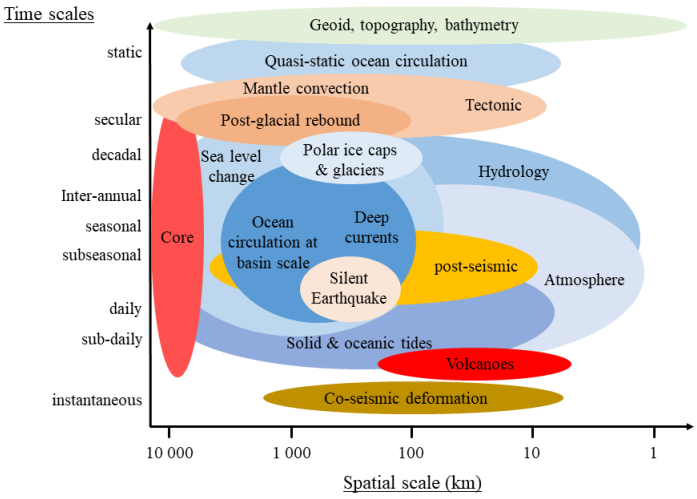

Figure 1: Spatial and temporal scales of the physical processes causing mass variations in the Earth system *adapted from Ilk et al. (2004)*

One way to extract the Earth's core signal from gravity observations is to use independent information from models of shallower sources (i.e. water mass redistribution in the hydrosphere, ocean, atmosphere, cryosphere and solid Earth's processes associated with earthquakes and glacial isostatic adjustment) to remove such larger amplitude contributions and to study the remaining signal. In this paper, we propose different models of post-glacial rebound, hydrological, atmospheric and oceanic mass redistribution for this purpose. The main

objective of this work is to estimate the uncertainty associated with each category of models at large spatial scales over 1200 km and inter-annual time scales to compare with the expected gravitational signature of some core processes. This estimation can not be done for the earthquakes and for the cryosphere because the existing models are not independent from GRACE observations (Deggim et al., 2021; Adhikari et al., 2016).

To our knowledge, there was no published study evaluating gravity field products and models at these scales. A first paper in this direction has assessed the accuracy of satellite laser ranging (SLR) and hydrological loading products at inter-annual time-scales and for degree-2 as compared with surface deformation from GNSS (Rosat et al., 2021). They showed that the gravity and surface deformation signatures of inter-annual degree-2 pressure flows at the CMB are much lower than the observed uncertainties.

Here we focus on the gravitational signature induced by various core processes that are firstly presented (2). We then present the spherical harmonics (SH) products and geophysical models used to estimate gravity variations (3). A minimum threshold of uncertainty is provided for each category of products and models (4). These uncertainties are finally discussed and compared with expected amplitudes of the presented core processes (5).

2 Expected gravitational signals from the Earth's core

Dynamical core processes disturb the time-varying gravity field through the direct Newtonian effect of mass anomalies in the fluid core. Dynamical core processes also have indirect effects, such as pressure changes at the CMB induced by varying core flows or changes in the rotation vector of the solid Earth. Dumberry and Mandea (2021) provided a review of the surface deformation and gravity variations induced by core dynamics, as well as a quantification of the expected amplitudes. In this part, we aim to provide a brief summary of these effects and an estimation of the amplitude in Equivalent Water Height (EWH) at the temporal scales observable with GRACE.

2.1 Spherical Harmonics (SH) representation

In the following, we note $C_{l,m}$ and $S_{l,m}$ the degree-l, order-m fully normalized Stokes coefficients of the SH representation of the Earth's gravitational potential. With $\hat{C}_{l,m}$ and $\hat{S}_{l,m}$ the unnormalized coefficients and $\delta_{m,0}$ the Kronecker delta, the normalization is given by:

$$\begin{bmatrix} C_{l,m} \\ S_{l,m} \end{bmatrix} = \sqrt{\frac{(n+m)!}{(2-\delta_{m,0})(2n+1)(n-m)!}} \begin{bmatrix} \hat{C}_{l,m} \\ \hat{S}_{l,m} \end{bmatrix} \tag{1}$$

The amplitude of the Stokes coefficient can be represented as EWH. An EWH amplitude, $\Delta\sigma(\lambda,\phi)$ is function of the longitude λ and the latitude ϕ (Wahr et al., 1998):

$$\Delta\sigma(\lambda,\phi) = \frac{R\bar{\rho}}{3\rho_w} \sum_{l=0}^{\infty} \sum_{m=0}^{l} \frac{2l+1}{1+k_l} \left[\Delta C_{l,m}\cos(m\lambda) + \Delta S_{l,m}\sin(m\lambda)\right] \bar{P}_l^m(\cos\phi), \tag{2}$$

where $\bar{P}_l^m(\cos\phi)$ are the associated fully normalized Legendre polynomials (4π normalization). R is the Earth's radius (6.371×10^6 m), $\bar{\rho}$ is the mean density of the Earth (5515 $kg.m^{-3}$), ρ_w is the density of water (1000 $kg.m^{-3}$) and k_l is the load Love number of degree l.

2.2 Newtonian effect of mass anomalies in the fluid core

Core flows create redistribution of density anomalies (Dumberry, 2010a). This first perturbation leads to an adjustment in the internal stress field. A secondary density perturbation is then created because of a global elastic deformation, due to this stress field.

A density perturbation, $\Delta\rho(r,\lambda,\phi)$ is function of the radius r, the longitude λ and the latitude ϕ. There is an expansion in SH for each radius r :

$$\Delta\rho(r,\lambda,\phi) = \sum_{l=0}^{\infty} \sum_{m=0}^{l} \left[\rho_{l,m}^c(r)\cos(m\lambda) + \rho_{l,m}^s(r)\sin(m\lambda)\right] \bar{P}_l^m(\cos\phi) \tag{3}$$

The gravity variation created by this density perturbation can be expressed as a SH coefficient variation of the gravity field, $\Delta C_{l,m}$ or $\Delta S_{l,m}$, by integrating the density perturbation for each radius in the fluid core between the Inner Core Boundary (ICB) and the CMB (Dumberry, 2010a).

$$\Delta C/S_{l,m} = \frac{4\pi}{2l+1} \frac{1}{MR^l} \int_{r_{ICB}}^{r_{CMB}} \rho_{l,m}^{c/s}(r)[1+\kappa_l(r)]r^{l+2}\mathrm{d}r, \tag{4}$$

where M corresponds to the mass of the Earth (5.972×10^{24} kg) and $\kappa_l(r)$ characterize the additional contribution due to global elastic deformation at degree l and radius r. $\kappa_l(r)$ values comes from Dumberry (2010a) and for degree $l > 2$, they fall within the range of approximately 0.2 and -0.2.

To have an order of amplitude of the gravitational effect created by density anomalies, we can take upper bound values for the density variations. The amplitude of density variations

within the Earth's core increases with the time scale of the analysis. This is because longer time scales allow for the observation of larger and more gradual changes in the density of the core, such as those caused by large-scale convection patterns (Dehant et al., 2022). At decadal and inter-annual time scales (maximal time-length achievable, yet, with GRACE observations), the upper bound of the density variation is $\Delta\rho = 1{\times}10^{-5}\ kg.m^{-3}$ (Dumberry & Mandea, 2021). For an annual period, this amplitude is smaller by one order of magnitude.

Supposing as an upper bound a variation with an amplitude of $\Delta\rho = 1{\times}10^{-5}\ kg.m^{-3}$ at each radius of the fluid core, we compute the effect for degree $l = 2$, 6 and 10. At inter-annual and decadal time scales, this gives respective Stokes coefficient variations of $2{\times}10^{-11}$, $1{\times}10^{-13}$ and $4{\times}10^{-15}$. This values can be estimated in cm EWH and for degree 2, 6 and 10, we respectively obtain as upper-bound values 0.1, 0.006 and 0.0005 cm EWH, over a decadal period.

2.3 Pressure flows effect

Besides the direct Newtonian effect, core flows create a tension on the CMB. This tension results in elastic deformations of the boundary and therefore, density perturbation (Dumberry, 2010a; Dumberry & Bloxham, 2004a). The same process occurs at the ICB.

In the same way as for density perturbation, we can describe the pressure anomalies $\Delta p(\lambda, \phi)$ with an expansion in SH at the CMB :

$$\Delta p(\lambda,\phi) = \sum_{l=0}^{\infty}\sum_{m=0}^{l}\left[p^{c}_{l,m}(r)\cos(m\lambda) + p^{s}_{l,m}(r)\sin(m\lambda)\right]\bar{P}^{m}_{l}(\cos\phi) \tag{5}$$

The gravity variations created by these pressure anomalies can be expressed as a SH coefficient variation of the gravity field $\Delta C_{l,m}$ or $\Delta S_{l,m}$ (Dumberry, 2010a) :

$$\Delta C/S_{l,m} = \bar{k_l}\ \frac{R}{GM\bar{\rho}}\ \ p^{c/s}_{l,m}(r), \tag{6}$$

where G is the gravitational constant ($6.674{\times}10^{-11}\ m^3kg^{-1}s^{-2}$) and $\bar{k_l}$ are potential Love numbers corresponding to degree l. For degree 2, 6 and 10, $\bar{k_l}$ values are respectively 1.116×10^{-1}, 1.957×10^{-3} and 9.856×10^{-5} (Dumberry & Mandea, 2021).

To have an order of amplitude of the gravitational effect created by pressure anomalies, we can use typical pressure variations. As for the density, the pressure amplitude is dependent on the period. As the time scale of the analysis increases, the amplitude of the pressure variations also increases (Gillet et al., 2020). At decadal and inter-annual time scales,

the typical pressure variations at the CMB should be $\Delta p = 100$ Pa (Dumberry & Mandea, 2021). For annual period, this amplitude is one order of magnitude smaller.

Supposing as an upper bound a variation with an amplitude of $\Delta p = 100$ Pa at the CMB, we compute the effect for degree $l = 2$, 6 and 10. At inter-annual and decadal time scales, this gives Stokes coefficient variations of 3×10^{-11}, 6×10^{-13} and 3×10^{-14} and corresponding EWH of 0.5, 0.04 and 0.004 cm EWH, over a decadal period.

2.4 Specific effects on degree 2 of the gravity field

We have previously discussed two mechanisms responsible for generating mass variations at different length scales. However, there are processes like alteration of the rotation vector and inner core reorientation that also lead to degree 2 variations :

2.4.1 Rotation effects of the core

Core dynamics can cause variations in the gravitational field through the alteration of the rotation vector of the solid Earth. For example, the exchange of angular momentum between the core and mantle produces changes in the angular velocity of the Earth, also express as Length of Day (LOD) variations. Pressure flows are responsible for decadal LOD variations (Jault & Finlay, 2015). Because Earth's angular momentum must be conserved, a change in the Earth's oblateness ($J_2 = -\sqrt{5}C_{2,0}$) is associated with a change in rotation. A 50 Pa change in $p_{2,0}$ at decadal periods result in $J_2 \approx 8\times10^{-12}$ (Gillet et al., 2020). This corresponds to $C_{2,0} \approx 4 \times 10^{-12}$ and 0.06 cm EWH.

A similar computation for the inner core rotation creates a variation of $C_{2,0}$ term that is five orders of magnitude lower (Dumberry & Bloxham, 2004b). It can then be ignored.

2.4.2 Inner Core reorientation

The inner core is supposed to have a topography at degree 2 and order 2, $h_{2,2}$. When the inner core is tilted by an angle α, it creates a variation on the coefficient $S_{2,2}$. This variation can be approximated by :

$$\Delta S_{2,2} \approx 10^{-10} h_{2,2} \alpha \tag{7}$$

under the hypothesis of a non-convecting inner core and with a density almost uniform at hydrostatic equilibrium (Dumberry, 2010b).

Dumberry and Mandea (2021) estimated the amplitude of the inner core reorientation supposing $\alpha = 0.4^o$ and $h_{2,2} = 18$ m on decadal time period. It gives $\Delta S_{2,2} = 10^{-11}$ and 0.2 cm EWH.

2.5 Summary of the gravitational signals from the Earth's core

The table 1 presents the amplitude of mass variations due to various core processes at different degree in EWH. The amplitude observed by GRACE is at least one order of magnitude larger than the predicted effects. Density anomalies have the lowest amplitude at degree 2 (0.1 cm EWH) and strongly decrease as the degree increases. These results suggest that mass variations due to core processes are most prominent at small degrees, and strongly decrease at higher degrees.

This observation is consistent with Rosat et al. (2021), which reports that at spherical harmonic degree 2, the contribution of core processes to gravity variations and ground deformations is approximately 10 times smaller than the observed fluctuations caused by dynamical processes within the fluid layers at the Earth' surface.

Table 1: Decadal amplitude of mass variations due to core processes at different degree in cm EWH

	EWH (cm)		
Gravitational effect	Degree 2	Degree 6	Degree 10
Amplitude observed by GRACE	5	20	15
Density anomalies	0.1	0.006	0.0005
CMB Pressure anomalies	0.5	0.04	0.004
Inner core rotation	0.2	X	X

This section points out that the study of the Earth's core trough gravity field variations can, yet, only be done at large spatial scales and inter-annual / decadal time scales. Consequently,

identifying signals of core origin poses a significant challenge and requires accurate removal of all surface effects.

3 Data presentation

Solutions for the time-variable gravity field are obtained using GRACE measurements with SLR measurements for low degrees. Geophysical models representing hydrological, oceanic and glacial isostatic adjustment (GIA) processes are obtained from independent models and not from GRACE inputs.

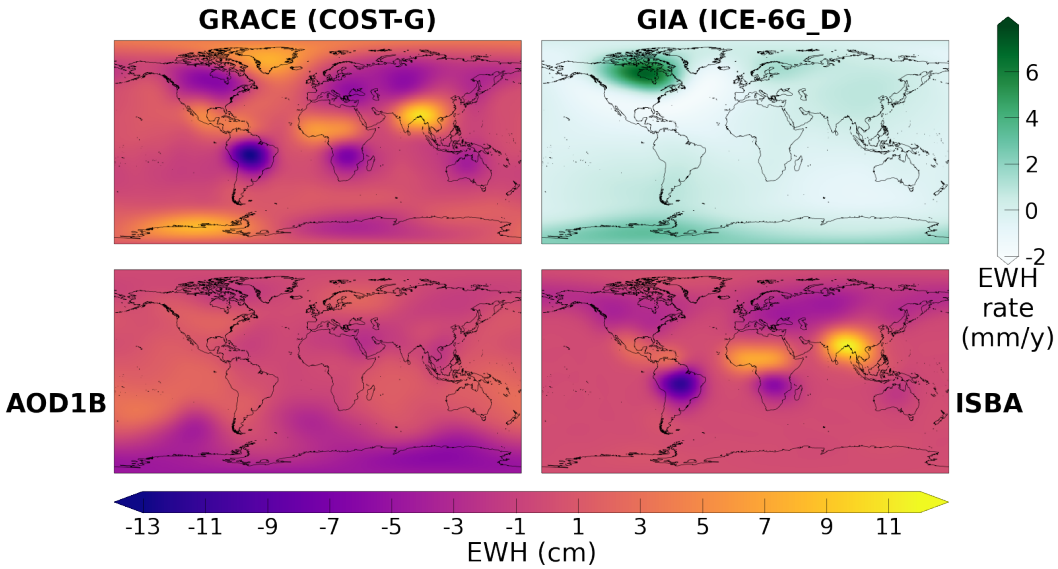

Figure 2: Surface mass in September 2008 estimated with the GRACE solution from the COST-G center (top left panel), the atmospheric and oceanic circulation model AOD1B (bottom left panel), the hydrological model Interaction Sol-Biosphère-Atmosphère (ISBA) (bottom right model) and GIA rate height change from ICE-6G_D (VM5a) model; a spatial filtering as detailed in 3.1

3.1 Mathematical approach

Models and solutions are provided in either spherical harmonics (SH) or grid representation (Swenson & Wahr, 2002). Since we are interested in large spatial scales, we primarily use SH processing and representation. We only use the grid format to represent our results

in a geographically interpretable way. Spatial representations are presented in Equivalent Water Height (EWH) (Fig. 2).

To study hypothetical gravity variations originating from the Earth's core, we filter the products and models considered in this study at appropriate spatial and temporal scales (Section: 2.5). The spatial filtering is done with a Gaussian filter (Jekeli, 1981) of radius 1200 km to access large spatial scales and avoid Gibbs aliasing. We do not use the usual isotropic spatial filter (Kusche, 2007) that allows to recover high resolution signals. Post-filtered SH are increasingly reduced to degree 12 because of the Gaussian filter (Fig. 3). The temporal filtering is done with a Butterworth low-pass filter with a cut-off period at 2 years. This removes high-amplitude signals with annual and semi-annual periods in the products and models.

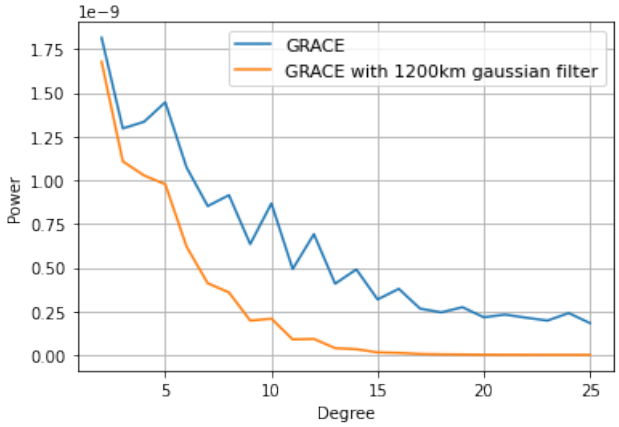

Figure 3: Power of SH degree for GRACE with and without spatial filtering up to degree 25

3.2 GRACE

GRACE gravity-field SH solutions are distributed by several analysis centers, providing GRACE Satellite-only Model (GSM) coefficients of the geopotential (Bettadpur, 2018). In this study, we considered 6 GSM solutions (see 2 for details) from the 3 Science Data System centers (Center for Space Research (CSR) (*CSR RL6.0*, 2018), German Research Centre for Geosciences (GFZ) (Dahle et al., 2019) and Jet Propulsion Laboratory (JPL) (*JPL RL6.0*, 2018)) and 3 non-official centers (International Combination Service for Time-variable Gravity Fields (COST-G) (Meyer et al., 2020), Institute of Geodesy at

Graz University of Technology (IFG-TU GRAZ) (Mayer-Gürr et al., 2018) and Centre national d'études spatiales (CNES) (Lemoine et al., 2019)). GRAZ and CNES centers propose different approaches: sub-monthly hydrological de-aliasing for GRAZ, addition of SLR inputs for low degree determination for CNES. COST-G is a combination of the solutions from the other 5 centers used in this paper with the addition of Astronomical Institute University Bern (AIUB) solution. Detailed information about considered solutions are given in Table 2.

The 6 GRACE solutions considered in this study have a quasi-monthly time resolution. Time series span from the start of the GRACE mission, April 2002, to April 2021. There is a gap of one year between mid-2017 and mid-2018 between the GRACE and the GRACE-FO missions. As we are interested in the low degrees of the gravity field variations, we use only spherical harmonics (SH) models and not MASCON products. SH solutions are global whereas MASCON products are designed to access higher spatial resolution with pre-established grid that are an a priori of the mass distribution (Scanlon et al., 2016). Others institutes propose GRACE solutions, but they are not considered here.

Table 2: Characteristics of the GRACE gravity-field models

Model	Mean Gravity Field Model	Ocean Tides	Atmospheric mass variations	Oceanic non-tidal mass variations	Data sources	Reference
CSR RL06	GGM05C	GOT4.8	AOD1B RL06 GAA	AOD1B RL06 GAB	`https://podaac-tools.jpl.nasa.gov/drive/`	(*CSR RL6.0*, 2018)
GFZ RL06	GGM05C	FES2014b	AOD1B RL06 GAA	AOD1B RL06 GAB	`https://podaac-tools.jpl.nasa.gov/drive/`	(Dahle et al., 2019)
JPL RL06	EIGEN-6C4	FES2014	AOD1B RL06 GAA	AOD1B RL06 GAB	`https://podaac-tools.jpl.nasa.gov/drive/`	(*JPL RL6.0*, 2018)
ITSG-Grace2018	ITSG-GraceGoce2017	FES2014b + GRACE estimates	AOD1B RL06 GAA and LSDM for sub-monthly hydrology de-aliasing	AOD1B RL06 GAB	`https://icgem.gfz-potsdam.de/`	(Mayer-Gürr et al., 2018)
CNES RL05	EIGEN-GRGS.RL04.MEAN-FIELD	FES2014b	3-D ECMWF ERA-Interim + AOD1B RL06 GAA	TUGO + AOD1B RL06 GAB	`https://grace.obs-mip.fr/`	(Lemoine et al., 2019)
COST-G RL01	X	X	X	X	`https://icgem.gfz-potsdam.de/`	(Meyer et al., 2020)

The $C_{2,0}$ estimation with GRACE data is affected by a disturbing 161-day periodic signal (Chen et al., 2005; Cheng & Ries, 2017) without a consensual explanation for this

issue. It has then become a standard to replace the GRACE determination of $C_{2,0}$ by the SLR one. We use the Technical notes TN14 solution based on SLR data and recommended in Loomis et al. (2019a). The GRACE $C_{3,0}$ is also poorly observed when the satellites pair is operating without two fully functional accelerometers (Loomis et al., 2020). The TN14 solution also provides a $C_{3,0}$ estimation that we include after October 2016 (GRACE month > 178). These two problematic estimations are suspected to also affect other coefficients such as $C_{4,0}$, $C_{5,0}$ and $C_{6,0}$ (Cheng & Ries, 2017; Sośnica et al., 2015; Loomis et al., 2020). However, the quality of these GRACE coefficients is comparable with the quality of the SLR coefficient estimation (Cheng & Ries, 2017; Velicogna et al., 2020). It seems then not relevant to replace these coefficients. Dahle et al. (2019) suggested to have a special attention to $C_{2,1}$ and $S_{2,1}$ coefficients that contain an anomaly correlated with a failure of the accelerometers. We choose to replace these two coefficients with the SLR solution from Cheng et al. (2011) after October 2016. These replacements are not included in the CNES solution because it already includes SLR data at low degrees. Geocenter coefficients $C_{1,0}$, $C_{1,1}$ and $S_{1,1}$ are not included in our data and are set to 0 for the CNES solution where they come from SLR.

Previous studies provided estimates of the uncertainty of GRACE products from different centers, but not at large spatial and inter-annual time scales. For example, Kvas et al. (2019) compared the GRAZ solution with those from CSR, GFZ and JPL in terms of temporal Root Mean Square (RMS) over a grid, quiet RMS time series and 161-day signal. Wang et al. (2021); Dobslaw et al. (2020) compared the estimations of global mean ocean mass and mean barystatic sea level with solutions from different centers. Blazquez et al. (2018) compared the trends of the global water budget components from 5 GRACE centers. It also estimated the uncertainties associated with the processing parameters, namely, the geocentre motions, $C_{2,0}$, filtering, leakage and GIA. Another estimation of the GRACE products uncertainty can be given by the RMS value over ocean but it has not been proposed, yet, for inter-annual time scales (Chen et al., 2021). It is also worth noting that MASCON products can be useful in error assessment (Loomis et al., 2019b). In the following, we compare GIA, hydrology and non-tidal oceanic models.

3.3 Glacial Isostatic Adjustment (GIA)

The GIA signal induces linear trends in the gravity field variations. Effects of the post-glacial rebound are apparent in Antarctica, Northern America and Scandinavia. This

signal rectification uses GIA models based on global ice-loading history and mantle viscosity. We do not consider regional GIA models since they would give spurious estimates of the GIA signal out of the specific regions for which they have been designed (Whitehouse et al., 2012). Present-day ice melting is not taken into account in the post-glacial rebound models, it hence constitutes another source of uncertainty.

We compare three different global GIA models, namely A13 (Geruo et al., 2013), ICE-6G_D (VM5a) (Peltier et al., 2015, 2018) and Caron18 (Caron et al., 2018).

A13 is based on the ICE5G ice-loading history model (Peltier, 2004) and on the multilayered viscosity profile VM2 (Peltier, 2004). A13 is computed via a 3-D finite-element method that creates a 3-D viscosity structure. ICE-6G_D (VM5a) uses an update of ICE5G ice-load history with the addition of GNSS vertical rates constraints and Antarctica ice height change data (Argus et al., 2014). ICE-6G_D (VM5a) includes a more recent viscosity profile VM5a. Caron18 represents the mean of an ensemble of 128,000 forward models calculated in a Bayesian framework. For each run model, the viscosity structure and the scaling coefficients for the ice-load history of the Australian National University (ANU) model (Lambeck et al., 2010, 2014) vary. The final Caron18 GIA is a weighting of each model inferred by the probabilistic information and contains an estimate of the uncertainty from the dispersion between the models. A synthesis of these models is available in Table 3.

Table 3: Main characteristics of the GIA models

Model	Ice History	Viscosity Model (VM)	Lateral Heterogeneity	GNSS data
A13	ICE5G	VM2	Yes	No
ICE-6G_D	ICE6G	VM5a	No	Yes
Caron18	From ANU	Bayesian mean VM	No	Yes

Comparisons between these three GIA models already exist, mainly with regard to the uplift rates as measured by GNSS and the viscosity profiles. Argus et al. (2014) and Peltier et al. (2015) compare ICE-6G_D with A13 respectively on Antarctica and North America. Caron et al. (2018) and Argus et al. (2021) compare ICE-6G_D with Caron18

on North America. It is worth noting that the closest model to the measured GNSS uplift rate is ICE-6G_D.

Global GIA models are not associated with any uncertainty except for Caron18 and studies rarely discuss that point (Caron et al., 2018; Melini & Spada, 2019). A way of estimating the impact of the uncertainty of those models is by comparing some of them for a specific application. Śliwińska et al. (2021) used two different GIA models to estimate polar motion while Blazquez et al. (2018) compared three GIA models for the determination of global ocean mass change and sea level budget. In the case of regional applications, Kappelsberger et al. (2021) compared three global and two regional models with the uplift estimation from GNSS on the north-east of Greenland. However, to the best of our knowledge, there is no comparative study of GIA models based on the SH approach that was published, and more specifically, on low SH degrees.

3.4 Hydrology

We compare five global hydrological models, namely the Global Land Data Assimilation System Noah 2.1 (GLDAS) (Rodell et al., 2004), ERA5 (Hersbach et al., 2020), WaterGAP Global Hydrology Model version 2.2d (WGHM) (Döll et al., 2003), Interaction Sol-Biosphère-Atmosphère CNRM version of TRIP (ISBA-CTRIP, further referred to as ISBA) (Decharme et al., 2019) and Hydrological Land Surface Discharge Model (LSDM) (Dill, 2008). Hydrological models contain mainly annual and semi-annual signals. With the temporal and spatial filtering to access the core-like scales, the residuals studied are small compared to the original signals. For example, the RMS value of ISBA over continent is 3.64 cm in EWH and 1.47 cm EWH after temporal filtering. These residuals contain climatic modes like El Niño-Southern Oscillation.

The five hydrological models considered solve the vertical water mass balance but only three of them also solve the lateral fluxes. The water mass balance is expressed as the Terrestrial Water Storage (TWS) anomaly.

For GLDAS, the permanently ice-covered areas have been masked out. GLDAS has a spatial resolution of 0.25^o per 0.25^o and a temporal resolution of 3 hours. ERA5 has the same temporal and spatial resolutions. ERA5 is the new global model from Copernicus Climate Change Service that replaces the ERA-Interim reanalysis (Dee et al., 2011). GLDAS uses Global Precipitation Climatology Centre (GPCC) V1.3 Daily Analysis (Adler et al.,

2003) has precipitation model. GPCC is a family of precipitation models based on in situ raingauge data to estimate monthly precipitation. For these two models, gravitational potential changes induced by hydrological mass redistribution and loading are computed as detailed in Petrov and Boy (2004) and Gégout et al. (2010).

WGHM, ISBA and LSDM are also supplemented with lateral fluxes solving. We use the variant IRR100 of WGHM forced with GPCC monthly V7.0 precipitation (Schneider et al., 2016). The output of the WGHM that we use in this study was already at a monthly-averaged temporal scale and the spatial resolution is 0.5^o. ISBA-CTRIP is the combination of a water balance model (ISBA) with a runoff model (CTRIP). ISBA has a temporal resolution of 3 hours and a spatial resolution of 1^o and it also uses GPCC V6 as a precipitation model. LSDM has a daily temporal frequency and a spatial resolution of 1^o. LSDM has been designed for large spatial scale geodetic applications such as the study of Earth's polar motion (Dill et al., 2010; Jin et al., 2012). Among the three models, only WGHM includes human-induced effects of freshwater resources. This contribution is extremely important when accounting for the contribution of freshwater fluxes to the global ocean (Schmied et al., 2020).

Table 4: Characteristics of the hydrological models

Acronym	Precipitation model	Sampling period	Space resolution
ERA5	Simultaneously generate	1 h	0.25^o
GLDAS	GPCP	3 h	0.25^o
ISBA	GPCC	3 h	1^o
WGHM	GPCC	monthly average	0.5^o
LSDM	ECMWF	daily	1^o

Each models has been resampled to a monthly time scale with an average over the month. The time coverage of comparison goes from 2002 to the end of 2016, this corresponds to the end of the WGHM model provided to us.

Previous studies compared hydrological models with GRACE gravity field variations but not with this diversity of models and not at these inter-annual and large spatial scales

(Lenczuk et al., 2020; Jin & Feng, 2013; Liu et al., 2019). At inter-annual and decadal scales, hydrological models compared with GRACE solution are underestimating the hydrological signal on river basins and regarding climate modes (Scanlon et al., 2018; Pfeffer et al., 2021, 2022).

3.5 Non-tidal oceanic loading

We compare three oceanic loading models, namely Ocean Model for Circulation and Tides (OMCT) (Dobslaw et al., 2013), Max-Planck-Institute for Meteorology Ocean Model (MPIOM) (Jungclaus et al., 2013) and Toulouse Unstructured Grid Ocean model (T-UGOm) (Carrere & Lyard, 2003). These models are used in GRACE solutions to correct for oceanic loading effects. For official centers, these models correspond to the GAB solution that contains the contribution of the dynamic ocean to ocean bottom pressure. OMCT has been used by official GRACE centers between Releases 1 and 5. MPIOM is used for the Release 6. T-UGOm is used by the CNES for the correction of the GRACE data (and not for GRACE-FO).

OMCT and MPIOM are baroclinic ocean models with a spatial resolution of 1^o. They are adjustments from another model, the climatological Hamburg Ocean Primitive Equation (HOPE) model. They are forced by external information from the operational analyses of the European Centre for Medium-Range Weather Forecast (ECMWF). They compute water elevations, three-dimensional horizontal velocities, potential temperature and salinity. Both MPIOM and OMCT are forced by surface winds, pressure, atmospheric freshwater fluxes and surface temperature. MPIOM is using river runoff, sea-ice and corrects for the inverted barometer response of the oceans as opposed to OMCT. The T-UGOm barotropic ocean model is based on an unstructured grid with a higher resolution on coastal area. It does not represent variations of temperature and salinity but only displacement of the barotropic fluid. T-UGOm is using wind and atmospheric pressure forcing from ERA-interim and does not correct the inverted barometer response. Temporal and spatial resolutions of each model are detailed in Table 5.

To compare these three models we can not use the GAB solutions from GRACE releases because of the difference in the correction of the inverted barometer effect. The GAB solution for AOD1B RL06 with MPIOM uses the correction of the inverted barometer effect. It implies that the AOD1B RL06 GAA solution, which corresponds to the atmospheric

Table 5: Characteristics of the ocean models

Acronym	Sampling period	Spatial resolution	Inverted barometer
OMCT	90 min	1^o	No
MPIOM	20 min	1^o	Yes
T-UGOm	3 hours	unstructured grid	No

loading effect, is equal to a constant value over oceanic area. For OMCT and T-UGOm, the GAB solution contains the inverted barometer effect and the GAA solution does not contain the inverted barometer effect. Regarding this, we compare the GAC solutions which are in fact the sum of the GAB (ocean loading) and the GAA (atmospheric loading) solutions over the ocean. This sum over oceanic areas corresponds to the oceanic bottom pressure and is given by the GAD solution in GRACE releases. To compare these oceanic loading models, the best way is to use the related GAD solutions.

Previous studies compared these models but at sub-monthly time scales (Bonin & Save, 2019; Dobslaw et al., 2015). To our knowledge, there are no comparative studies of ocean loading models on inter-annual and decadal temporal scales. Schindelegger et al. (2021) also compared some other oceanic models with MPIOM at sub-monthly time scales. We did not include these other models because some are in-house products and other are GRACE-dependent.

4 Comparison of gravity field solutions and models

In our approach, we cannot directly estimate the accuracy of solutions and models. We use an ensemble approach where the dispersion between solutions and models provides an estimate of the uncertainty. This estimate is a first lower bound that does not take into account any bias. This approach is similar to Blazquez et al. (2018) or Marti et al. (2022).

Comparisons between solutions and models are quantified as the Root Mean Square (RMS) difference between both objects weighted by latitude. In order to compute the weighted RMS, solutions and models are projected on a grid of $0.5^o \times 0.5^o$ degree and we compute the difference between the grids.

4.1 Differences between GRACE solutions

4.1.1 GRACE analysis centers

Comparison between GRACE solutions requires to minimize side effects due to the temporal filtering. We hence remove the first and last three months of the solutions.

	JPL	GFZ	GRAZ	CNES	COSTG	RMS
CSR	**0.17**	**0.35**	**0.32**	**0.45**	**0.16**	**1.82**
JPL		**0.32**	**0.31**	**0.45**	**0.16**	**1.81**
GFZ			**0.45**	**0.53**	**0.30**	**1.82**
GRAZ				**0.45**	**0.27**	**1.87**
CNES					**0.42**	**1.86**
COSTG						**1.81**

Table 6: RMS differences in cm EWH between different GRACE solutions and RMS value of each model after spatial and temporal filtering

Table 6 contains the RMS differences in cm EWH between the spatially and temporally filtered GRACE solutions from different analysis centers. For reference, the RMS value of the CSR solution is 1.82 cm EWH. The first group, CSR, JPL and COST-G solutions, is the most similar with an RMS difference of 0.16-0.17 cm EWH or 9% of the original RMS value for one solution. There is an increase of the difference to 0.22 cm EWH in 2016 at the end of GRACE lifespan corresponding to the accelerometer failure of one of the two satellites. Then comes a second group with GFZ and GRAZ which have an RMS difference of 0.3 cm EWH with the first group or 17% of the original RMS value for one solution. But the difference of these two solutions with the first group is different according to the considered epoch. GFZ has a peak going up to 0.7 cm EWH at the end of the GRACE lifespan. For GRAZ, in this temporal period, the difference goes up to 0.5 cm EWH but then it goes to 0.7 cm EWH at the end of the GRACE-FO time series. For the GFZ, the spatial distribution of differences corresponds to a global noise without any specific pattern. But for the GRAZ solutions, differences are located in areas of large signals, in the Amazon basin and Greenland. The CNES solution has a RMS difference of 0.45 cm EWH (25%

433 of the original RMS value) with respect to other solutions with a temporal difference of
434 1 cm EWH at the beginning of the GRACE mission and at the end of the GRACE life
435 span. The spatial localisation of these differences are located in areas of strong hydrological
436 signal like the Amazon basin and India. Figures to illustrate these analyses are available
437 in Appendix A.

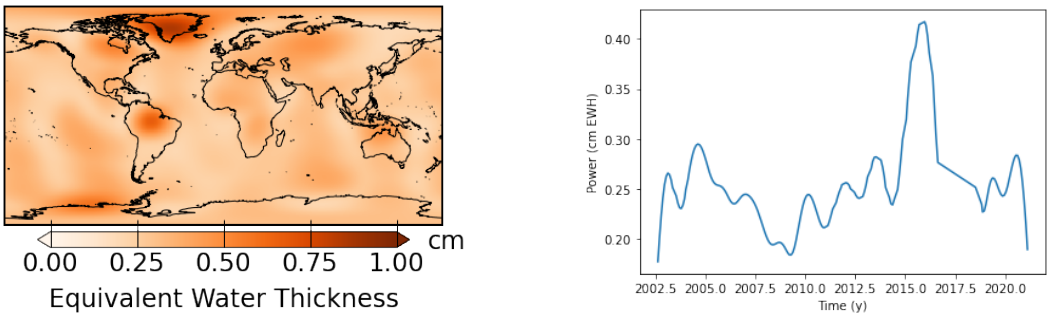

(a) Average of RMS differences in cm EWH spatially represented

(b) Average of RMS differences in cm EWH represented trough time

Figure 4: Average of RMS differences in cm EWH after spatial and temporal filtering

438 To continue the analysis of the differences between the GRACE solutions, it is important
439 to consider the average RMS values over time and in different spatial areas (Fig. 4). The
440 highest values over Greenland, Antarctica and Amazonia correspond spatially to areas
441 with strong inter-annual signals. Thus, the stronger the signal, the larger the differences
442 between the solutions. For the temporal variations of the RMS differences between solutions,
443 the difference are twice larger at the end of the GRACE mission. The degradation of the
444 quality of GRACE solutions is well known and has already been documented (Kvas et
445 al., 2019; Dahle et al., 2019). This degradation is due to the failure of the accelerometer
446 after November 2016 and is smoothed trough time in Figure 4b because of the temporal
447 filtering. Otherwise, the RMS values over time are about 0.25 cm in EWH.

448 ### *4.1.2 GIA models*

449 Figure 5 represents the difference in rate of EWH in mm per year between the models
450 with a spatial resolution of 2400 km after a truncation at degree 60 and the application
451 of a Gaussian filter. In Appendix B, the same figure without spatial filtering is available.

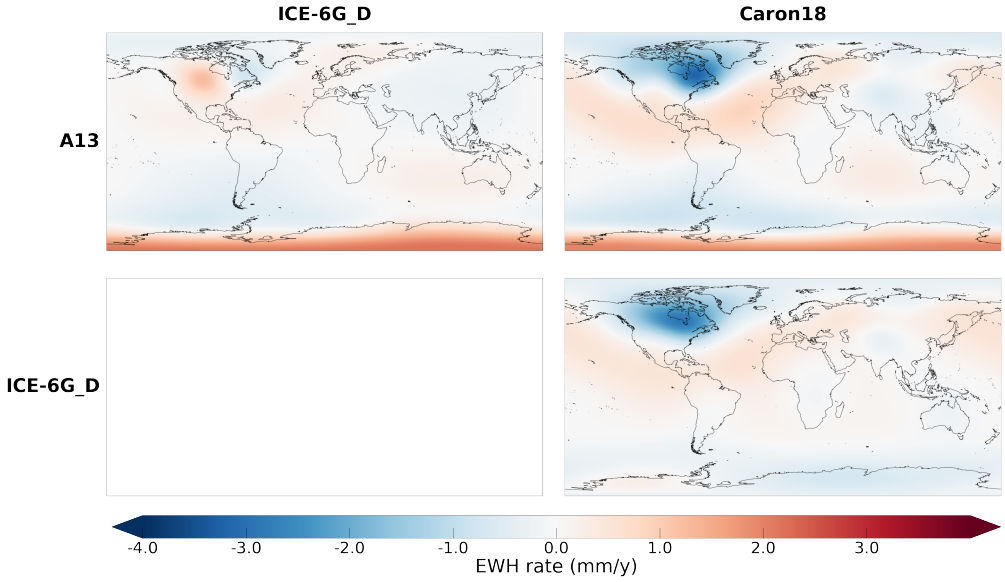

Figure 5: Difference between GIA models spatially filtered in EWH rate (mm/y)

The models are similar in Scandinavia. The Caron18 model differs from the others in North America and the A13 model differs from the others in Antarctica. These two statements correspond to previous observations (Argus et al., 2021, 2014). There are small differences between A13 and the ICE-6G_D model in North America (±1 mm/y in EWH) compared to those in Antarctica (±3 mm/y). Peltier et al. (2015) pointed out a larger difference on the western and eastern sides of Hudson Bay in Canada that we recovered without the spatial filtering (Appendix B). However, in Figure 5, the spatial filtering reduces these differences, one being negative and the other positive, they counterbalance each other.

In North America, the disagreement between models goes up to 6 mm in EWH per year. In Antarctica, the differences between models are up to 10 mm in EWH per year. These differences in velocity are currently accumulated over 20 years and at the time of publication of this article, they lead to a potential error of 12 cm in EWH per year over North America and of 20 cm in EWH per year over Antarctica.

4.1.3 Hydrological models

Table 7 contains the RMS differences in cm EWH between spatially and temporally filtered hydrological loading models (Newtonian attraction and mass redistribution associated

	GLDAS	ISBA	WGHM	LSDM	RMS
ERA5	**0.89**	**0.89**	**1.36**	**1.50**	**0.91**
GLDAS		**0.89**	**1.20**	**1.74**	**1.26**
ISBA			**1.13**	**1.56**	**1.00**
WGHM				**2.10**	**1.36**
LSDM					**1.66**

Table 7: RMS difference in cm EWH between hydrological models and RMS value of each model after spatial and temporal filtering over the continents

with elastic deformation) over continents without Greenland and Antarctica. The RMS difference goes from 0.89 to 2.10 cm EWH or 100% to 155% of the original RMS value for one model. For example, the RMS values of ISBA and LSDM are respectively 1.00 and 1.66 cm EWH.

Because hydrological models take into account different processes, they yield very different TWS anomalies, leading to large differences in the predicted gravity variations at large spatial and temporal scales. At inter-annual and large spatial scales, ERA5, GLDAS and ISBA display relatively similar signals (Fig. 6a). Probably because it takes into account anthropogenic use of freshwater, WGHM exhibits larger differences, with larger TWS changes at inter-annual signals located in India and in the northern hemisphere than the other models (Fig. 6c).

LSDM shows the largest difference with other models. It has a very strong signal over the Nile area in North Africa (Fig. 6b). The difference between LSDM and other hydrological models like GLDAS has been documented and explained by the particular river channels redistribution of water (Dill & Dobslaw, 2013; Dill et al., 2018).

The same analysis has been done on hydrological loading model without spatial filtering in Appendix C1.

The quality of hydrological loading models is uneven. To evaluate this quality we look at the percentage of RMS explained by the models in the variation of the gravity field. We compare, over the continents, the RMS of the GRACE time series (COST-G)

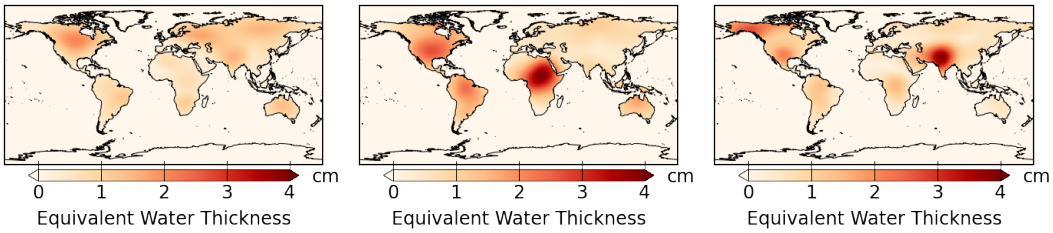

(a) ERA5 minus GLDAS

(b) ISBA minus LSDM

(c) ISBA minus WGHM

Figure 6: Maps of RMS difference between hydrological models over the continents after spatial and temporal filtering

with the RMS of GRACE minus a hydrological model. The variation of the RMS value gives the percentage of RMS explain by the model in the GRACE time series (Table 8) over non-glaciated continents (Greenland and Antartica are not include).

	ERA5	GLDAS	ISBA	WGHM	LSDM
Percentage (%)	7	0	24	21	-16

Table 8: Percentage of RMS explain by hydrological models in the GRACE time series at inter-annual scales with a spatial filtering over non-glaciated continents

At inter-annual and large spatial scales, ISBA and WGHM reduce the variance of GRACE solutions by more than 20%. According to this criteria they have the best quality among the five models considered. ERA5 and GLDAS are close to 0% and LSDM is negative with -16%. It does not modelize gravity field variations in GRACE time-series and contains other signals. Global hydrological models struggle to explain GRACE data, likely due to inaccurate meteorological forcing, unresolved groundwater processes, anthropogenic influences, changing vegetation cover, limited calibration and validation datasets (Pfeffer et al., 2022).

	MPIOM	T-UGOm	RMS
OMCT	**0.33**	**0.45**	**0.42**
MPIOM		**0.42**	**0.39**
T-UGOm			**0.44**

Table 9: RMS difference in cm EWH between oceanic loading products and RMS value of each model after spatial and temporal filtering over the oceans

4.1.4 Non-tidal oceanic loading models

Table 9 contains the RMS differences in cm EWH between spatially and temporally filtered oceanic and atmospheric loading products over the oceans. The RMS difference goes from 0.33 to 0.45 cm EWH between models or 79% to 107% of the original RMS value for one model. For comparison, the RMS value for OMCT is 0.42 cm EWH. Because oceanic loading models come from different climate and fluid mechanics models, they have a very different spatial and temporal content, leading to large differences. Differences are mostly located in Arctic and Antarctic areas, coastal regions and in the Antarctic Circumpolar Current area (Fig. 7). OMCT has more signal in the Arctic while MPIOM and T-UGOm have more signal near Antarctica in the Ross Sea (Fig. 7).

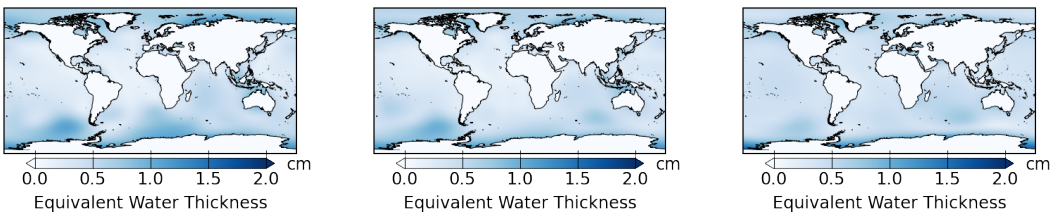

(a) OMCT (b) MPIOM (c) T-UGOm

Figure 7: Maps of RMS for oceanic loading products after spatial and temporal filtering over the oceans

There is another difference between these models: they are monthly products with potential missing days each month. These missing days correspond to low quality data

but may vary between models and releases. This is the case for months at the beginning and at the end of the GRACE mission in 2002 and between 2012 and 2017. For example, for the month of August 2016, the MPIOM products from official centers contain measurements from days of year 221 to 247 while the T-UGOm products from the CNES contain measurements from days of year 214 to 244.

The same analysis has been done for oceanic loading models without spatial filtering (Appendix D1).

4.2 Impact of geophysical corrections on Stokes coefficients

We have quantified the uncertainties of GRACE solutions and correction models in terms of RMS of the differences over grids. Another interesting approach is to look at SH coefficients. Core processes signal might be present from degree 2 onward to higher degrees with decreasing amplitudes.

To estimate the impact of an error in a model on specific SH coefficients, we have performed some synthetic test. An artificial synthetic signal is added to the GRACE gravity data on a bounded area. We choose these synthetic signals with regard to the observed errors in the GIA and hydrological loading models. We study the effects of this synthetic signal on the retrieved Stokes coefficients in terms of RMS value. To compare with the time-variable gravity measured by GRACE, we normalized each SH coefficients by the standard deviation $\sigma_{l,m}^{GRACE}$ of the degree-l, order-m Stokes coefficient from the COST-G solution. We note $I_{l,m}$ the normalized RMS value of the coefficient of degree l and order m given by:

$$I_{l,m} = \frac{\sqrt{\frac{1}{n}\sum_{t} \Delta C_{l,m}(t)^2}}{\sigma_{l,m}^{GRACE}} \tag{8}$$

With t the index of the time vector. This representation gives an estimate of the contamination by an error on the correction model with respect to the corrected GRACE signal.

4.2.1 Impact of an error in the GIA model

To study the effect of adding a fiducial GIA rectification, we create three synthetic signals corresponding to errors seen in 4.1.2.

- A linear signal of 10 mm/y in EWH located in North America with latitude between 50^o and 70^o and longitude between -95^o and -65^o.
- A linear signal of 6 mm/y in EWH located in Antarctica with latitude under -80^o.
- A linear signal of 3 mm/y in EWH located in Antarctica with latitude under -70^o and longitude between -160^o and -30^o.

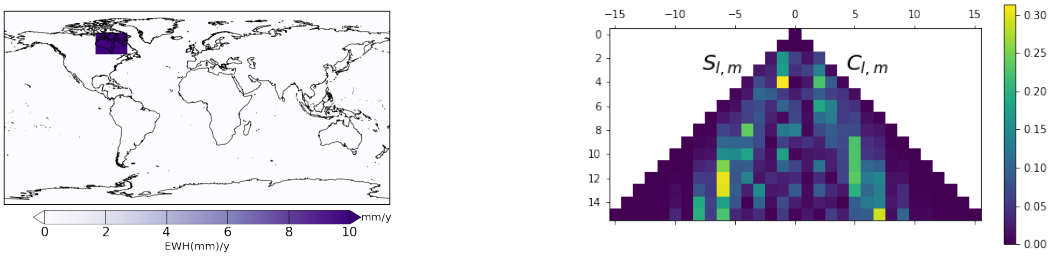

(a) Synthetic signal in North America in EWH

(b) SH power normalized by GRACE standard deviation up to degree 15

Figure 8: Effect of a 10 mm/yr trend in North America in the GIA model (a) on GRACE SH coefficients (b).

Introducing a 10 mm/y trend in North America alters the SH coefficients (Fig. 8). The error created on the GRACE $S_{4,1}$ coefficient by this fiducial reduction might be up to 30%. The other two synthetics experiments, with a trend at lower latitudes, affect the coefficients of orders 0 and 1 (Appendix E). The largest effect for a trend of 6 mm/y over Antarctica center is on $C_{8,0}$ with a trended bias of 50% of the GRACE RMS value. For a 3 mm/y trend in Antarctica between -160^o and -30^o in longitude, the effects are smaller with 15% of the GRACE RMS value on $S_{6,1}$ and $S_{8,1}$ (Appendix E).

4.2.2 Hydrology

Three cases have been simulated with a sinusoidal signal of period 3 years. They correspond to the difference between hydrological models established in Figure 6 over large hydrological basins:

- A sinusoidal signal of 4 cm in EWH over Africa (latitude between -10^o and 10^o, longitude between 10^o and 35^o).

- A sinusoidal signal of 3 cm in EWH over Amazonia (latitude between 0^o and 20^o, longitude between -70^o and -40^o).
- A sinusoidal signal of 4 cm in EWH over India (latitude between 20^o and 30^o, longitude between 70^o and 90^o).

The 3-year period was chosen arbitrarily and represents a residual hydrological signal.

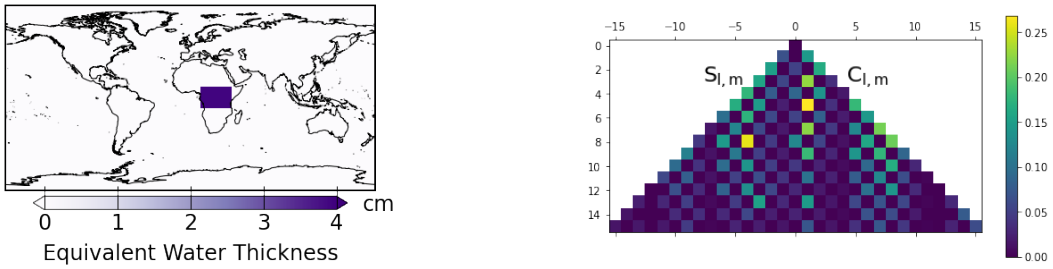

(a) Synthetic 3-yr signal over Africa with an amplitude of 4 cm EWH

(b) SH power normalized by GRACE standard deviation up to degree 15

Figure 9: Effect of a sinusoidal signal over Africa (a) on GRACE SH coefficients (b)

A 4-cm sinusoidal signal over Africa affects $C_{5,1}$ and $S_{8,4}$ by an amount of 25% of the GRACE RMS value (Fig. 9). A 3 cm sinusoidal signal over Amazonia affects $C_{4,3}$ and $S_{2,2}$ by an amount of 20%, while a 4 cm signal over India affects $C_{8,7}$ and $S_{8,6}$ by an amount of 10% (Appendix F).

5 Discussions & Conclusions

In this paper, we firstly addressed different core processes that can create gravity variation and estimated their amplitudes. Then, we presented different GRACE SH solutions, GIA and loading models. We compared each family of products with respect to the differences in RMS or trend at large spatial and inter-annual time scales. From this, we estimated their uncertainties and the associated SH uncertainties.

A summary of the orders of magnitude of predicted core signals and of the dispersion between the different solutions and models obtained in this article is given in Table 10. It contains the amplitude of the RMS difference at degrees 2, 6 and 10. The largest core signals amplitude with regard to the uncertainty is found at degree 2. At degrees 6 and

	(cm EWH)	Amplitude (cm EWH)		
Type of data	Mean RMS difference	Degree 2	Degree 6	Degree 10
Maximum of the estimated core signals	0.5	0.5	0.04	0.004
GRACE solutions	0.34	X	0.1	0.04
Hydrological loading models	1.32	0.37	0.38	0.41
Oceanic loading models	0.40	0.16	0.08	0.03

Table 10: Amplitude of core estimated signals compared to RMS difference between products at inter-annual and large spatial scales and at degrees 2, 6 and 10

10, the amplitude estimated from core signals is an order of magnitude smaller than the estimated uncertainty of the GRACE solutions. To summarize the information on amplitude from this table:

- Mass variations from the core are characterized by their low degree signature and by an inter-annual / decadal time scale. The maximal amplitude of core effects is evaluated at 0.5 cm EWH which is slightly larger than the estimated GRACE uncertainty at inter-annual and large spatial scales.
- GRACE solutions are in good agreement with a dispersion that represents some 10 to 20% of the total signal, however, the agreement is not the same over the time span covered by the two missions, with difference meanly at the beginning and end of each.
- For hydrological loading models, the agreement is uneven (see also Fig. 6 & Table 7, 8). The dispersion between models is a large as the RMS value of models themselves. However, ISBA and WGHM are closer to GRACE solutions.
- For the oceanic loading models, the agreement is generally poor (see also Fig. 7). For each model, high-intensity signals are spatially located in different areas at inter-annual time scales. For example, T-UGOm is the only model to report large oceanic mass variations under South Africa.
- The GIA effects are not included in this recapitulating table as they are localized in specific areas: North America, Greenland and Antartica. To remind, GIA-mismodelled

linear effects can go up to a 20 cm EWH after 20 years over North America. GIA errors will only impact the trend and not the inter-annual signals.

When models characterising surface processes are considered to minimise the signature of these processes in the gravity data, they might indeed create some spurious signals on some areas. This would also create a spurious signal on specific SH (Fig. 8, Fig. 9) up to 50% of the total signal on inter-annual time scale.

The estimated maximum amplitude of core signals based on a literature review is 5 mm in EWH at the Earth's surface. Core mass variations are most significant on decadal time scales and at low degrees. In this context, it is relevant to analyse the Earth's gravity products from GRACE and loading models trough these specific scales. The RMS difference between GRACE solutions of 3.4 mm in EWH shows how difficult is to detect potential core signals. This difficulty is somehow reinforced when considering the use of loading models to minimize these components in the gravity signal, as the differences between loading products are large and these products are not completely adapted to our purpose.

A careful analysis of the time-variable gravity field data needs to be done for detecting signals from the core processes. Firstly, the data-gap between GRACE and GRACE-FO should be filled to ensure continuity and to improve the products quality (Richter et al., 2021). The largest signals in GRACE-kind solutions are due to the Earth's surface processes. The inter-annual variability analysis through climate modes (Pfeffer et al., 2021) needs also to be considered. In order to detect tiny signals related to the core more sophisticated methods are needed such as empirical orthogonal function analysis (Schmeer et al., 2012) or independent component analysis (Frappart et al., 2011). Recently, (Saraswati et al., 2022) applied Singular Value Decomposition (SVD), Principal Component Analysis (PCA) and Multivariate Singular Spectrum Analysis (MSSA) to separate distinct spatio-temporal patterns in magnetic and gravity field. Moreover, synthetic tests have to be performed to evaluate the sensitivity of these methods with respect of the Earth's core signals.

Both gravity and magnetic fields are complex, with a wide range of temporal and spatial variations and to describe them new models are needed. Only by modelling and interpreting multiple data sets a multifaceted image of the true structure of the Earth can be obtained.

6 Supplementary materials

Appendix A Temporal variation of the RMS difference between various GRACE solutions

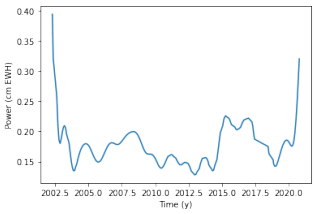

(a) Temporal RMS difference between CSR and JPL solutions

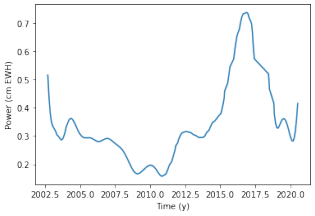

(b) Temporal RMS difference between CSR and GFZ solutions

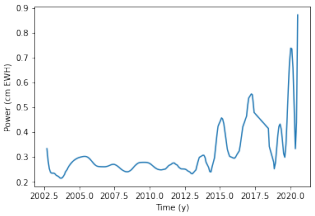

(c) Temporal RMS difference between CSR and GRAZ solutions

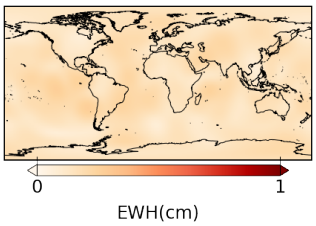

(d) Spatial RMS difference between CSR and JPL solutions

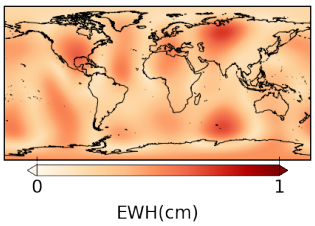

(e) Spatial RMS difference between CSR and GFZ solutions

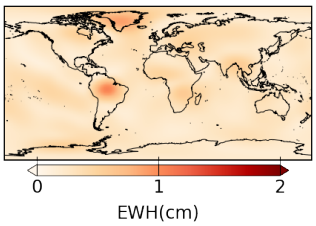

(f) Spatial RMS difference between CSR and GRAZ solutions

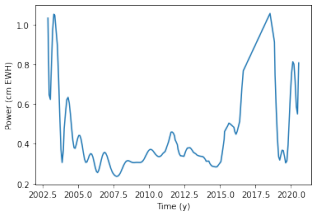

(g) Temporal RMS difference between CSR and CNES solutions

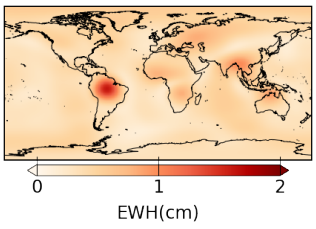

(h) Spatial RMS difference between CSR and CNES solutions

Figure A1: RMS difference between GRACE center solutions on temporal and spatial representation

Appendix B Difference between GIA models without spatial filtering

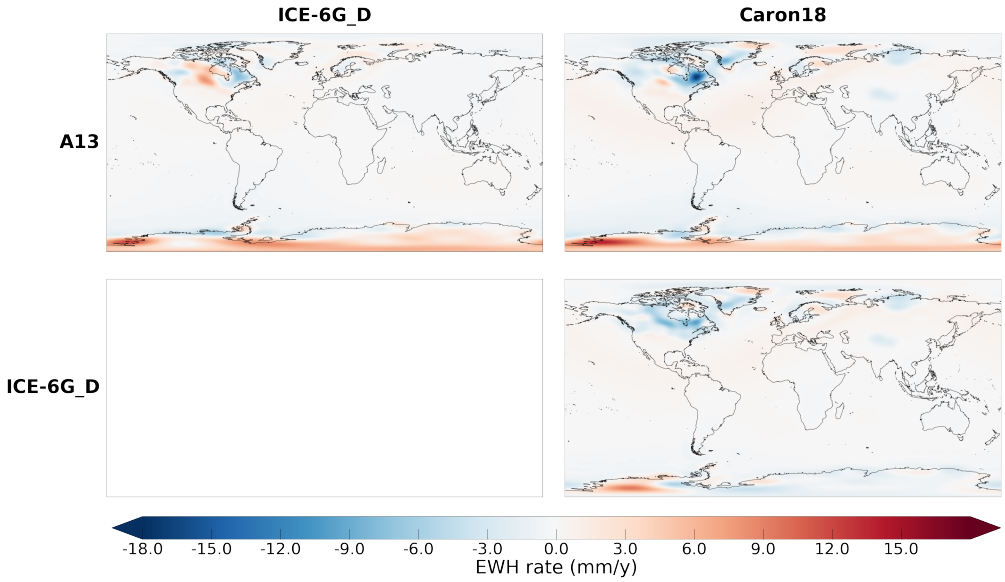

Figure B1: Difference of between GIA models in EWH rate (mm/y)

The amplitude of the GIA signal is five times larger without spatial filtering and the signal is more localize.

Appendix C Difference between hydrological loading with temporal filtering and without spatial filtering

	GLDAS	ISBA	WGHM	LSDM	RMS
ERA5	**2.06**	**2.11**	**2.92**	**2.69**	**2.35**
GLDAS		**2.04**	**2.74**	**2.99**	**2.67**
ISBA			**2.55**	**2.66**	**2.43**
WGHM				**3.67**	**3.05**
LSDM					**2.47**

Table C1: RMS difference in cm EWH between hydrological models and RMS value of each model after a temporal filtering

Table C1 contains the RMS difference in cm EWH between temporally filtered hydrological models over continents without Greenland and Antarctica. The RMS difference goes from 2.04 to 3.67 cm EWH between models. For example of comparison, the RMS value of ISBA and WGHM are respectively 2.43 and 3.05 cm EWH.

At inter-annual time scales, the models show different signals. For example, WGHM is the only one to contain a strong signal over India and North America, while LSDM is the only one to contain a signal over the Nile region in Africa. They do not correspond at all.

We can also note that the spatial filtering smooths the signal amplitude.

Appendix D Difference between oceanic loading with temporal filtering and without spatial filtering

	MPIOM	T-UGOm	RMS
OMCT	**0.72**	**0.79**	**0.84**
MPIOM		**0.74**	**0.77**
T-UGOm			**0.52**

Table D1: RMS difference in cm EWH between oceanic loading solutions and RMS value of each model after temporal filtering

Table D1 contains the RMS difference in cm EWH between temporally filtered oceanic and atmospheric loading models over the oceans. The RMS difference goes from 0.72 to 0.79 cm EWH between models. For comparison, the RMS value for OMCT is 0.84 cm EWH. This means that models are not in agreement at inter-annual scales and they represent very different signals.

Appendix E Cases n^o2 and n^o3 for GIA synthetic error effects

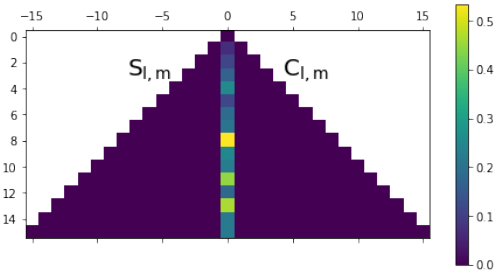

(a) Case n^o2 with synthetic signal under -80^o of latitude

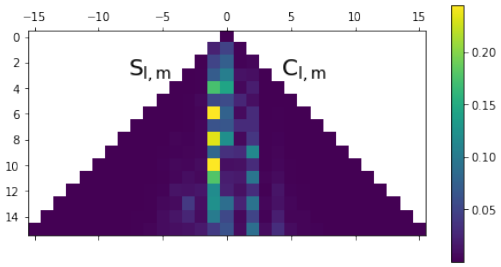

(b) Case n^o3 with synthetic signal under -70^o of latitude and between -160^o and -30^o of longitude

Figure E1: SH power normalized by GRACE standard deviation up to degree 15

Appendix F Cases n^o2 and n^o3 for synthetic error effects corresponding to hydrological loading

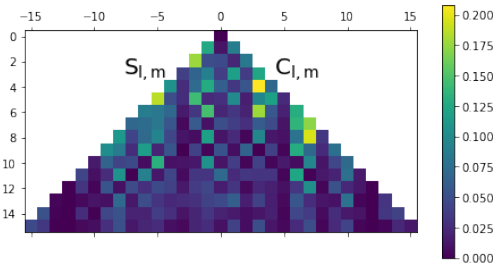

(a) Case n^o2 with synthetic signal over Amazon forest

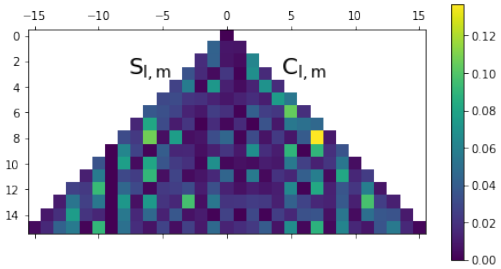

(b) Case n^o3 with synthetic signal over India

Figure F1: SH power normalized by GRACE standard deviation up to degree 15

Acronyms

AIUB Astronomical Institute University Bern

CMB Core-Mantle Boundary

CNES Centre national d'études spatiales

CSR Center for Space Research

EWH Equivalent Water Height

GFZ German Research Centre for Geosciences

GIA Glacial Isostatic Adjustment

GLDAS Global Land Data Assimilation System

GRACE Gravity Recovery And Climate Experiment

GRACE-FO Gravity Recovery And Climate Experiment Follow-On

GSM GRACE Satellite-only Model

IFG TU Graz Institute of Geodesy at Graz University of Technology

ISBA Interaction Sol-Biosphère-Atmosphère

ISBA-CTRIP Interaction Sol-Biosphère-Atmosphère CNRM version of TRIP

JPL Jet Propulsion Laboratory

MPIOM Max-Planck-Institute for Meteorology Ocean Model

OMCT Ocean Model for Circulation and Tides

RMS Root Mean Square

SH Spherical Harmonics

SLR Satellite Laser Ranging

T-UGOm Toulouse Unstructured Grid Ocean model

TWS Total Water Storage

WGHM WaterGAP Global Hydrology Model

Acknowledgments

This work is supported by the Centre national d'études spatiales (CNES) and by the Doctoral School Earth and Environmental Sciences (ED 413) of the University of Strasbourg in the Institut Terre et Environnement de Strasbourg (ITES, CNRS UMR7063). This project has received funding from the European Research Council (ERC) under the European Union's Horizon 2020 research and innovation program (GRACEFUL Synergy Grant agreement No 855677).

Love numbers and $\kappa(r)$ values to estimate Earth's core signals have been kindly provided by Mathieu Dumberry, we thank him for these inputs.

We thank the editor Paul Tregoning and the two referees for their valuable remarks which improved the first manuscript.

GRACE and GRACE-FO missions are sponsored by the National Aeronautics and Space Administration and the Deutsches Zentrum für Luft-und Raumfahrt. GRACE and GRACE-FO Level-2 temporal solutions were obtained from the PO.DAAC Drive for CSR, GFZ and JPL centers, from `https://icgem.gfz-potsdam.de/` for ITSG center, from `https://grace.obs-mip.fr/` for CNES center and from `https://icgem.gfz-potsdam.de/` for the COST-G combination. The GIA models were obtained from the PO.DAAC Drive (`http://grace.jpl.nasa.gov`). Time-variable gravity field coefficients due to hydrological loading can be downloaded from EOST loading service (`http://loading.u-strasbg.fr/`) for ERA5 and GLDAS models. LSDM model is available on the ESMGFZ Product repository (`http://rz-vm115.gfz-potsdam.de:8080`) and is produced by IERS Associated Product Centre Deutsches GeoForschungsZentrum GFZ Potsdam. The ISBA-CTRIP model made by the "Centre National de Recherches Météorologiques" (CNRM) of Méteo-France has been provided by Bertrand Descharmes. The WGHM model (`http://www.watergap.de/`) has been provided by Denise Caceres from Frankfurt University. MPIOM and OMCT are available on the PO.DAAC Drive and T-UGOm model has been provided by the CNES.

Finally, the Python 3.8 code used for this publication is based on a Github project by Tyler Tsutterley (`https://github.com/tsutterley/read-GRACE-harmonics`). The adapted version can be found on `https://github.com/hulecom/read-GRACE-harmonics` repository.

References

Adhikari, S., Ivins, E. R., Frederikse, T., Landerer, F. W., & Caron, L. (2019, May). Sea-level fingerprints emergent from GRACE mission data. *Earth System Science Data*, *11*(2), 629–646. Retrieved 2022-07-21, from `https://essd.copernicus.org/articles/11/629/2019/` (Publisher: Copernicus GmbH) doi: 10.5194/essd-11-629-2019

Adhikari, S., Ivins, E. R., & Larour, E. (2016, March). ISSM-SESAW v1.0: mesh-based computation of gravitationally consistent sea-level and geodetic signatures caused by cryosphere and climate driven mass change. *Geoscientific Model Development*, *9*(3), 1087–1109. Retrieved 2022-07-21, from `https://gmd.copernicus.org/articles/9/1087/2016/` doi: 10.5194/gmd-9-1087-2016

Adler, R. F., Huffman, G. J., Chang, A. T. C., Ferraro, R., Xie, P., Janowiak,

J. E., ... Nelkin, E. (2003). The version 2 global precipitation climatology project (gpcp) monthly precipitation analysis (1979-present). *Journal of Hydrometeorology*. doi: 10.1175/1525-7541(2003)004⟨1147:tvgpcp⟩2.0.co;2

Argus, D. F., Peltier, W. R., Blewitt, G., & Kreemer, C. (2021). The Viscosity of the Top Third of the Lower Mantle Estimated Using GPS, GRACE, and Relative Sea Level Measurements of Glacial Isostatic Adjustment. *Journal of Geophysical Research: Solid Earth*, *126*(5), e2020JB021537. Retrieved 2023-01-13, from `https://onlinelibrary.wiley.com/doi/abs/10.1029/2020JB021537` (_eprint: https://onlinelibrary.wiley.com/doi/pdf/10.1029/2020JB021537) doi: 10.1029/2020JB021537

Argus, D. F., Peltier, W. R., Drummond, R., & Moore, A. W. (2014, July). The Antarctica component of postglacial rebound model ICE-6G_c (VM5a) based on GPS positioning, exposure age dating of ice thicknesses, and relative sea level histories. *Geophysical Journal International*, *198*(1), 537–563. Retrieved 2023-01-12, from `https://doi.org/10.1093/gji/ggu140` doi: 10.1093/gji/ggu140

Bettadpur, S. (2018). *Level-2 Gravity Field Product User Handbook* (User Handbook). Center for Space Research. Retrieved from `https://podaac-tools.jpl.nasa.gov/drive/files/allData/grace/docs/L2-UserHandbook_v4.0.pdf`

Blazquez, A., Meyssignac, B., Lemoine, J.-M., Berthier, E., Ribes, A., & Cazenave, A. (2018). Exploring the uncertainty in GRACE estimates of the mass redistributions at the Earth surface: implications for the global water and sea level budgets. *Geophysical Journal International*. doi: 10.1093/gji/ggy293

Bonin, J. A., & Save, H. (2019). Evaluation of sub-monthly oceanographic signal in grace "daily" swath series using altimetry. *Ocean Science Discussions*. doi: 10.5194/os-16-423-2020

Bouih, M., Panet, I., Remy, D., Longuevergne, L., & Bonvalot, S. (2022). Deep mass redistribution prior to the 2010 mw 8.8 maule (chile) earthquake revealed by grace satellite gravity. *Earth and Planetary Science Letters*, *584*, 117465. Retrieved from `https://www.sciencedirect.com/science/article/pii/S0012821X22001017` doi: https://doi.org/10.1016/j.epsl.2022.117465

Caron, L., Ivins, E. R., Larour, E., Larour, E., Adhikari, S., Nilsson, J., ... Blewitt, G. (2018). Gia model statistics for grace hydrology, cryosphere, and ocean science. *Geophysical Research Letters*. doi: 10.1002/2017gl076644

Carrere, L., & Lyard, F. (2003). Modeling the barotropic response of the global ocean to atmospheric wind and pressure forcing - comparisons with observations. *Geophysical Research Letters*. doi: 10.1029/2002gl016473

Chen, J., Cazenave, A., Dahle, C., Llovel, W., Panet, I., Pfeffer, J., & Moreira, L. (2022, February). Applications and Challenges of GRACE and GRACE Follow-On Satellite Gravimetry. *Surveys in Geophysics*, *43*(1), 305–345. Retrieved 2022-07-21, from `https://doi.org/10.1007/s10712-021-09685-x` doi: 10.1007/s10712-021-09685-x

Chen, J., Rodell, M., Wilson, C. R., & Famiglietti, J. S. (2005). Low degree spherical harmonic influences on gravity recovery and climate experiment (grace) water storage estimates. *Geophysical Research Letters*. doi: 10.1029/2005gl022964

Chen, J., Tapley, B., Tamisiea, M. E., Save, H., Wilson, C., Bettadpur, S., & Seo, K.-W. (2021). Error Assessment of GRACE and GRACE Follow-On Mass Change. *Journal of Geophysical Research: Solid Earth*, *126*(9), e2021JB022124. Retrieved 2022-11-29, from `https://onlinelibrary.wiley.com/doi/abs/10.1029/2021JB022124` (_eprint: https://onlinelibrary.wiley.com/doi/pdf/10.1029/2021JB022124) doi: 10.1029/2021JB022124

Cheng, M., & Ries, J. C. (2017). The unexpected signal in grace estimates of c_{20}. *Journal of Geodesy*. doi: 10.1007/s00190-016-0995-5

Cheng, M., Ries, J. C., & Tapley, B. D. (2011). Variations of the earth's figure axis from satellite laser ranging and grace. *Journal of Geophysical Research*. doi: 10.1029/2010jb000850

CSR RL6.0. (2018). Retrieved from `https://podaac.jpl.nasa.gov/dataset/GRACE_GSM_L2_GRAV_CSR_RL06`

Dahle, C., Flechtner, F., Dobslaw, H., Michalak, G., Neumayer, K.-H., Reinhold, A., ... Sulzbach, R. (2019). The GFZ GRACE RL06 Monthly Gravity Field Time Series: Processing Details and Quality Assessment. *Remote Sensing*. doi: 10.3390/rs11182116

Decharme, B., Delire, C., Minvielle, M., Colin, J., Vergnes, J., Alias, A., ... Voldoire, A. (2019). Recent changes in the isba-ctrip land surface system for use in the cnrm-cm6 climate model and in global off-line hydrological applications. *Journal of Advances in Modeling Earth Systems*. doi: 10.1029/2018ms001545

Dee, D., Uppala, S., Simmons, A., Berrisford, P., Kobayashi, S., Andrae, U., ... Thépaut, J.-N. (2011). The era-interim reanalysis: configuration and performance of the data assimilation system. *Quarterly Journal of the Royal Meteorological Society*. doi: 10.1002/qj.828

Deggim, S., Eicker, A., Schawohl, L., Gerdener, H., Schulze, K., Engels, O., ... Longuevergne, L. (2021, May). RECOG RL01: correcting GRACE total water storage estimates for global lakes/reservoirs and earthquakes. *Earth System Science Data*, *13*(5), 2227–2244. Retrieved 2022-03-11, from `https://essd.copernicus.org/articles/13/2227/2021/` (Publisher: Copernicus GmbH) doi: 10.5194/essd-13-2227-2021

Dehant, V., Campuzano, S. A., De Santis, A., & van Westrenen, W. (2022, February). Structure, Materials and Processes in the Earth's Core and Mantle. *Surveys in Geophysics*, *43*(1), 263–302. Retrieved 2023-01-23, from `https://doi.org/10.1007/s10712-021-09684-y` doi: 10.1007/s10712-021-09684-y

Dill, R. (2008). Hydrological model lsdm for operational earth rotation and gravity field variations. *null*. doi: 10.2312/gfz.b103-08095

Dill, R., Dill, R., Dobslaw, H., & Dobslaw, H. (2010). Short-term polar motion forecasts from earth system modeling data. *Journal of Geodesy*. doi: 10.1007/s00190-010-0391-5

Dill, R., & Dobslaw, H. (2013). Numerical simulations of global-scale high-resolution hydrological crustal deformations. *Journal of Geophysical Research: Solid Earth*, *118*(9), 5008–5017. Retrieved 2022-06-23, from `https://onlinelibrary.wiley.com/doi/abs/10.1002/jgrb.50353` (_eprint: https://onlinelibrary.wiley.com/doi/pdf/10.1002/jgrb.50353) doi: 10.1002/jgrb.50353

Dill, R., Klemann, V., & Dobslaw, H. (2018). Relocation of River Storage From Global Hydrological Models to Georeferenced River Channels for Improved Load-Induced Surface Displacements. *Journal of Geophysical*

Research: Solid Earth, *123*(8), 7151–7164. Retrieved 2022-06-23, from https://onlinelibrary.wiley.com/doi/abs/10.1029/2018JB016141 (_eprint: https://onlinelibrary.wiley.com/doi/pdf/10.1029/2018JB016141) doi: 10.1029/2018JB016141

Dobslaw, H., Bergmann-Wolf, I., Dill, R., Poropat, L., Thomas, M., Dahle, C., ... Flechtner, F. (2017, October). A new high-resolution model of non-tidal atmosphere and ocean mass variability for de-aliasing of satellite gravity observations: AOD1B RL06. *Geophysical Journal International*, *211*(1), 263–269. Retrieved 2022-07-21, from https://doi.org/10.1093/gji/ggx302 doi: 10.1093/gji/ggx302

Dobslaw, H., Bergmann-Wolf, I., Forootan, E., Dahle, C., Mayer-Gürr, T., Kusche, J., & Flechtner, F. (2015). Modeling of present-day atmosphere and ocean non-tidal de-aliasing errors for future gravity mission simulations. *Journal of Geodesy*. doi: 10.1007/s00190-015-0884-3

Dobslaw, H., Dill, R., Dill, R., Bagge, M., Klemann, V., Boergens, E., ... Flechtner, F. (2020). Gravitationally consistent mean barystatic sea level rise from leakage-corrected monthly grace data. *Journal of Geophysical Research*. doi: 10.1029/2020jb020923

Dobslaw, H., Dobslaw, H., Flechtner, F., Bergmann-Wolf, I., Dahle, C., Dahle, C., ... Thomas, M. (2013). Simulating high-frequency atmosphere-ocean mass variability for dealiasing of satellite gravity observations: Aod1b rl05. *Journal of Geophysical Research*. doi: 10.1002/jgrc.20271

Dumberry, M. (2010a). Gravity variations induced by core flows. *Geophysical Journal International*, *180*(2), 635–650. Retrieved 2022-03-11, from https://doi.org/10.1111/j.1365-246X.2009.04437.x doi: 10.1111/j.1365-246X.2009.04437.x

Dumberry, M. (2010b, September). Gravitationally driven inner core differential rotation. *Earth and Planetary Science Letters*, *297*(3-4), 387–394. Retrieved 2022-10-25, from https://linkinghub.elsevier.com/retrieve/pii/S0012821X10004152 doi: 10.1016/j.epsl.2010.06.040

Dumberry, M., & Bloxham, J. (2004a). Variations in the Earth's gravity field caused by torsional oscillations in the core. *Geophysical Journal International*, *159*(2), 417–434.

Dumberry, M., & Bloxham, J. (2004b, November). Variations in the Earth's gravity field caused by torsional oscillations in the core. *Geophysical Journal International*, *159*(2), 417–434. Retrieved 2023-01-19, from https://doi.org/10.1111/j.1365-246X.2004.02402.x doi: 10.1111/j.1365-246X.2004.02402.x

Dumberry, M., & Mandea, M. (2021). Gravity Variations and Ground Deformations Resulting from Core Dynamics. *Surveys in Geophysics*. Retrieved 2022-03-11, from https://doi.org/10.1007/s10712-021-09656-2 doi: 10.1007/s10712-021-09656-2

Döll, P., Kaspar, F., & Lehner, B. (2003). A global hydrological model for deriving water availability indicators: model tuning and validation. *Journal of Hydrology*. doi: 10.1016/s0022-1694(02)00283-4

Frappart, F., Ramillien, G., Leblanc, M., Leblanc, M., Tweed, S., Bonnet, M.-P., & Maisongrande, P. (2011). An independent component analysis filtering approach for estimating continental hydrology in the grace gravity data. *Remote Sensing of Environment*. doi: 10.1016/j.rse.2010.08.017

Gégout, P., Boy, J.-P., Hinderer, J., & Ferhat, G. (2010). Modeling and observation of loading contribution to time-variable GPS sites positions. In *Gravity, geoid and earth observation* (pp. 651–659). Springer.

Geruo, A., Wahr, J., & Zhong, S. (2013). Computations of the viscoelastic response of a 3-D compressible Earth to surface loading: an application to Glacial Isostatic Adjustment in Antarctica and Canada. *Geophysical Journal International*. doi: 10.1093/gji/ggs030

Gillet, N., Dumberry, M., & Rosat, S. (2020). The limited contribution from outer core dynamics to global deformations at the Earth's surface. *Geophysical Journal International*, *224*, 216–229. doi: 10.1093/gji/ggaa448

Gillet, N., Gerick, F., Jault, D., Schwaiger, T., Aubert, J., & Istas, M. (2022, March). Satellite magnetic data reveal interannual waves in Earth's core. *Proceedings of the National Academy of Sciences*, *119*(13), e2115258119. Retrieved 2023-01-27, from https://www.pnas.org/doi/abs/10.1073/pnas.2115258119 (Publisher: Proceedings of the National Academy of Sciences) doi: 10.1073/pnas.2115258119

Gillet, N., Lesur, V., & Olsen, N. (2010, August). Geomagnetic Core Field Secular Variation Models. *Space Science Reviews*, *155*(1), 129–145. Retrieved 2022-05-06, from https://doi.org/10.1007/s11214-009-9586-6 doi: 10.1007/s11214-009-9586-6

Hersbach, H., Bell, B., Berrisford, P., Hirahara, S., Horanyi, A., Munoz-Sabater, J., ... Thépaut, J.-N. (2020). The era5 global reanalysis. *Quarterly Journal of the Royal Meteorological Society*. doi: 10.1002/qj.3803

Horwath, M., Gutknecht, B. D., Cazenave, A., Palanisamy, H. K., Marti, F., Marzeion, B., ... Benveniste, J. (2022, February). Global sea-level budget and ocean-mass budget, with a focus on advanced data products and uncertainty characterisation. *Earth System Science Data*, *14*(2), 411–447. Retrieved 2022-07-21, from https://essd.copernicus.org/articles/14/411/2022/ (Publisher: Copernicus GmbH) doi: 10.5194/essd-14-411-2022

Ilk, K.-H., Flury, J., Rummel, R., Schwintzer, P., Bosch, W., Haas, C., ... Gravity Field and Gravimetry 2009, G. C. (2004). *Mass Transport and Mass Distribution in the Earth System : Contribution of the New Generation of Satellite Gravity and Altimetry Missions to Geosciences; Proposal for a German Priority Research Program* (Tech. Rep.). Retrieved 2022-06-22, from https://gfzpublic.gfz-potsdam.de/pubman/faces/ViewItemFullPage.jsp?itemId=item_231104_1 (Publisher: GOCE-Projektbüro Deutschland, Techn. Univ. München, GeoForschungsZentrum Potsdam)

Jault, D., & Finlay, C. C. (2015, January). 8.09 - Waves in the Core and Mechanical Core–Mantle Interactions. In G. Schubert (Ed.), *Treatise on Geophysics (Second Edition)* (pp. 225–244). Oxford: Elsevier. Retrieved 2023-01-31, from https://www.sciencedirect.com/science/article/pii/B9780444538024001500 doi: 10.1016/B978-0-444-53802-4.00150-0

Jekeli, C. (1981). Alternative methods to smooth the earth's gravity field. *null*. doi: null

Jin, S., & Feng, G. (2013, July). Large-scale variations of global groundwater from satellite gravimetry and hydrological models, 2002–2012. *Global and Planetary Change*, *106*, 20–30. Retrieved 2022-06-23, from https://linkinghub.elsevier.com/retrieve/pii/S0921818113000416 doi: 10.1016/j.gloplacha.2013.02.008

Jin, S., Hassan, A. A., & Feng, G. (2012). Assessment of terrestrial water contributions to polar motion from grace and hydrological models. *Journal of Geodynamics*. doi: 10.1016/j.jog.2012.01.009

JPL RL6.0. (2018). Retrieved from `https://podaac.jpl.nasa.gov/dataset/GRACE_GSM_L2_GRAV_JPL_RL06`

Jungclaus, J. H., Fischer, N., Haak, H., Lohmann, K., Marotzke, J., Matei, D., ... von Storch, J.-S. (2013). Characteristics of the ocean simulations in mpiom the ocean component of the mpi earth system model. *Journal of Advances in Modeling Earth Systems*. doi: 10.1002/jame.20023

Kappelsberger, M. T., Strößenreuther, U., Scheinert, M., Horwath, M., Groh, A., Knöfel, C., ... Khan, S. A. (2021). Modeled and observed bedrock displacements in north-east Greenland using refined estimates of present-day ice-mass changes and densified GNSS measurements. *Journal of Geophysical Research*. doi: 10.1029/2020jf005860

Koelemeijer, P. (2021). Toward consistent seismological models of the core–mantle boundary landscape. In *Mantle convection and surface expressions* (p. 229-255). American Geophysical Union (AGU). Retrieved from `https://agupubs.onlinelibrary.wiley.com/doi/abs/10.1002/9781119528609.ch9` doi: https://doi.org/10.1002/9781119528609.ch9

Kusche, J. (2007). Approximate decorrelation and non-isotropic smoothing of time-variable grace-type gravity field models. *Journal of Geodesy*. doi: 10.1007/s00190-007-0143-3

Kusche, J., & Schrama, E. J. O. (2005). Surface mass redistribution inversion from global GPS deformation and Gravity Recovery and Climate Experiment (GRACE) gravity data. *Journal of Geophysical Research: Solid Earth*, *110*(B9). Retrieved 2022-07-21, from `https://onlinelibrary.wiley.com/doi/abs/10.1029/2004JB003556` (_eprint: https://onlinelibrary.wiley.com/doi/pdf/10.1029/2004JB003556) doi: 10.1029/2004JB003556

Kvas, A., Behzadpour, S., Ellmer, M., Klinger, B., Strasser, S., Zehentner, N., & Mayer-Gürr, T. (2019). Itsg-grace2018: Overview and evaluation of a new grace-only gravity field time series. *Journal of Geophysical Research: Solid Earth*, *124*(8), 9332-9344. Retrieved from `https://`

agupubs.onlinelibrary.wiley.com/doi/abs/10.1029/2019JB017415 doi: https://doi.org/10.1029/2019JB017415

Lambeck, K., Purcell, A. W., Zhao, J., Zhao, J., & Svensson, N.-O. (2010). The scandinavian ice sheet: from mis 4 to the end of the last glacial maximum. *Boreas*. doi: 10.1111/j.1502-3885.2010.00140.x

Lambeck, K., Rouby, H., Purcell, A. W., Sun, Y., & Sambridge, M. (2014). Sea level and global ice volumes from the last glacial maximum to the holocene. *Proceedings of the National Academy of Sciences of the United States of America*. doi: 10.1073/pnas.1411762111

Landerer, F. W., Flechtner, F. M., Save, H., Webb, F. H., Bandikova, T., Bertiger, W. I., ... Yuan, D.-N. (2020). Extending the Global Mass Change Data Record: GRACE Follow-On Instrument and Science Data Performance. *Geophysical Research Letters*, *47*(12), e2020GL088306. Retrieved 2022-07-21, from https://onlinelibrary.wiley.com/doi/abs/10.1029/2020GL088306 (_eprint: https://onlinelibrary.wiley.com/doi/pdf/10.1029/2020GL088306) doi: 10.1029/2020GL088306

Lemoine, J.-M., Biancale, R., Reinquin, F., Bourgogne, S., & Gégout, P. (2019). *CNES/GRGS RL04 Earth gravity field models, from GRACE and SLR data.* GFZ Data Services. Retrieved from https://dataservices.gfz-potsdam.de/icgem/showshort.php?id=escidoc:4656890 (Type: dataset) doi: 10.5880/ICGEM.2019.010

Lenczuk, A., Leszczuk, G., Klos, A., Kosek, W., & Bogusz, J. (2020, October). Study on the inter-annual hydrology-induced deformations in Europe using GRACE and hydrological models. *Journal of Applied Geodesy*, *14*(4), 393–403. Retrieved 2022-06-23, from https://www.degruyter.com/document/doi/10.1515/jag-2020-0017/html (Publisher: De Gruyter) doi: 10.1515/jag-2020-0017

Liu, R., She, D., Li, M., & Wang, T. (2019). Using satellite observations to assess applicability of gldas and wghm hydrological model. *Geomatics and Information Science of Wuhan University*, *44*(1671?8860(2019)11?1596?09), 1596. Retrieved from http://ch.whu.edu.cn/en/article/doi/10.13203/j.whugis20190108 doi: 10.13203/j.whugis20190108

Loomis, B. D., Luthcke, S. B., & Sabaka, T. J. (2019b, September). Regularization and error characterization of GRACE mascons. *Journal of Geodesy*, *93*(9), 1381–1398. Retrieved 2022-12-01, from https://doi.org/10.1007/s00190-019-01252-y doi: 10.1007/s00190-019-01252-y

Loomis, B. D., Rachlin, K. E., & Luthcke, S. B. (2019a). Improved earth oblateness rate reveals increased ice sheet losses and mass-driven sea level rise. *Geophysical Research Letters*. doi: 10.1029/2019gl082929

Loomis, B. D., Wiese, D. N., Landerer, F. W., Rachlin, K. E., & Luthcke, S. B. (2020). Replacing grace/grace-fo with satellite laser ranging: Impacts on antarctic ice sheet mass change. *Geophysical Research Letters*. doi: 10.1029/2019gl085488

Mandea, M., Narteau, C., Panet, I., & Le Mouël, J.-L. (2015). Gravimetric and magnetic anomalies produced by dissolution-crystallization at the core-mantle boundary. *Journal of Geophysical Research: Solid Earth*, *120*(9), 5983–6000. Retrieved 2022-03-11, from https://onlinelibrary.wiley.com/doi/abs/10.1002/2015JB012048 (_eprint: https://onlinelibrary.wiley.com/doi/pdf/10.1002/2015JB012048) doi: 10.1002/2015JB012048

Mandea, M., Panet, I., Lesur, V., de Viron, O., Diament, M., & Le Mouël, J.-L. (2012, November). Recent changes of the Earth's core derived from satellite observations of magnetic and gravity fields. *Proceedings of the National Academy of Sciences*, *109*(47), 19129–19133. Retrieved 2022-03-11, from https://www.pnas.org/doi/full/10.1073/pnas.1207346109 (Publisher: Proceedings of the National Academy of Sciences) doi: 10.1073/pnas.1207346109

Marti, F., Blazquez, A., Meyssignac, B., Ablain, M., Barnoud, A., Fraudeau, R., ... Benveniste, J. (2022, January). Monitoring the ocean heat content change and the Earth energy imbalance from space altimetry and space gravimetry. *Earth System Science Data*, *14*(1), 229–249. Retrieved 2022-07-21, from https://essd.copernicus.org/articles/14/229/2022/ (Publisher: Copernicus GmbH) doi: 10.5194/essd-14-229-2022

Mayer-Gürr, T., Behzadpour, S., Ellmer, M., Klinger, B., Zehentner, N., Kvas, A., & Strasser, S. (2018). Itsg-grace2018: Monthly, daily and static gravity field

solutions from grace. *null*. doi: 10.5880/icgem.2018.003

Melini, D., & Spada, G. (2019). Some remarks on Glacial Isostatic Adjustment modelling uncertainties. *Geophysical Journal International*. doi: 10.1093/gji/ggz158

Meyer, U., Lasser, M., Jaeggi, A., Dahle, C., Dahle, C., Flechtner, F., ... Bourgogne, S. (2020). International combination service for time-variable gravity fields (cost-g) monthly grace-fo series. *null*. doi: 10.5880/icgem.cost-g.002

Panet, I., Bonvalot, S., Narteau, C., Remy, D., & Lemoine, J.-M. (2018, May). Migrating pattern of deformation prior to the Tohoku-Oki earthquake revealed by GRACE data. *Nature Geoscience*, *11*(5), 367–373. Retrieved 2022-03-11, from `https://www.nature.com/articles/s41561-018-0099-3` (Number: 5 Publisher: Nature Publishing Group) doi: 10.1038/s41561-018-0099-3

Peltier, W. R. (2004). Global glacial isostasy and the surface of the ice-age earth: The ice-5g (vm2) model and grace. *Annual Review of Earth and Planetary Sciences*. doi: 10.1146/annurev.earth.32.082503.144359

Peltier, W. R., Argus, D. F., & Drummond, R. (2015). Space geodesy constrains ice age terminal deglaciation: The global ICE-6G_C (VM5a) model. *Journal of Geophysical Research*. doi: 10.1002/2014jb011176

Peltier, W. R., Argus, D. F., & Drummond, R. (2018). Comment on "An Assessment of the ICE-6G_C (VM5a) Glacial Isostatic Adjustment Model" by Purcell et al. *Journal of Geophysical Research*. doi: 10.1002/2016jb013844

Petrov, L., & Boy, J.-P. (2004). Study of the atmospheric pressure loading signal in VLBI observations. *Journal of Geophysical Research*, *109*(B03405).

Pfeffer, J., Cazenave, A., & Barnoud, A. (2021). Analysis of the interannual variability in satellite gravity solutions: detection of climate modes in water mass displacements across continents and oceans. *Climate Dynamics*. doi: 10.1007/s00382-021-05953-z

Pfeffer, J., Cazenave, A., Blazquez, A., Decharme, B., Munier, S., & Barnoud, A. (2022, December). Detection of slow changes in terrestrial water storage with GRACE and GRACE-FO satellite gravity missions. *EGUsphere*, 1–85. Retrieved 2023-01-27, from `https://egusphere.copernicus.org/preprints/2022/egusphere-2022-1032/` (Publisher: Copernicus GmbH)

doi: 10.5194/egusphere-2022-1032

Purcell, A., Dehecq, A., Tregoning, P., Potter, E.-K., McClusky, S. C., & Lambeck, K. (2011). Relationship between glacial isostatic adjustment and gravity perturbations observed by GRACE. *Geophysical Research Letters*, *38*(18). Retrieved 2022-03-11, from `https://onlinelibrary.wiley.com/doi/abs/10.1029/2011GL048624` (_eprint: https://onlinelibrary.wiley.com/doi/pdf/10.1029/2011GL048624) doi: 10.1029/2011GL048624

Richter, H. M. P., Lück, C., Klos, A., Sideris, M. G., Rangelova, E., & Kusche, J. (2021). Reconstructing GRACE-type time-variable gravity from the Swarm satellites. *Scientific Reports*, *11*. Retrieved from `https://doi.org/10.1038/s41598-020-80752-w` doi: 10.1038/s41598-020-80752-w

Rodell, M., Famiglietti, J. S., Wiese, D. N., Reager, J. T., Beaudoing, H. K., Landerer, F. W., & Lo, M.-H. (2018, May). Emerging trends in global freshwater availability. *Nature*, *557*(7707), 651–659. Retrieved 2022-07-21, from `https://www.nature.com/articles/s41586-018-0123-1` (Number: 7707 Publisher: Nature Publishing Group) doi: 10.1038/s41586-018-0123-1

Rodell, M., Houser, P., Jambor, U., Gottschalck, J., Mitchell, K., Meng, C.-J., ... others (2004). The global land data assimilation system. *Bulletin of the American Meteorological Society*, *85*(3), 381–394.

Rosat, S., Gillet, N., Boy, J.-P., Couhert, A., & Dumberry, M. (2021, February). Interannual variations of degree 2 from geodetic observations and surface processes. *Geophysical Journal International*, *225*(1), 200–221. Retrieved 2022-03-11, from `https://doi.org/10.1093/gji/ggaa590` doi: 10.1093/gji/ggaa590

Saraswati, A. T., de Viron, O., & Mandea, M. (2022, June). *Estimation des signaux communs de la gravité spatiale et du champ magnétique liés à la variation du champ du noyau terrestre* [Poster]. Congrès national de gravimétrie spatiale du champ variable, Marseille. Retrieved 2022-07-27, from `https://gravimetriefr.sciencesconf.org/browse/session?sessionid=71661`

Scanlon, B. R., Zhang, Z., Save, H., Sun, A. Y., Schmied, H. M., Beek, L. P. H. v., ... Bierkens, M. F. P. (2018, February). Global models underestimate large decadal declining and rising water storage trends relative to GRACE satellite

data. *Proceedings of the National Academy of Sciences*, *115*(6), E1080–E1089. Retrieved 2021-07-29, from https://www.pnas.org/content/115/6/E1080 (Publisher: National Academy of Sciences Section: PNAS Plus) doi: 10.1073/pnas.1704665115

Scanlon, B. R., Zhang, Z., Save, H., Wiese, D. N., Landerer, F. W., Long, D., ... Chen, J. (2016). Global evaluation of new grace mascon products for hydrologic applications. *Water Resources Research*, *52*(12), 9412-9429. Retrieved from https://agupubs.onlinelibrary.wiley.com/doi/abs/10.1002/2016WR019494 doi: https://doi.org/10.1002/2016WR019494

Schindelegger, M., Harker, A., Ponte, R. M., Dobslaw, H., & Salstein, D. A. (2021). Convergence of daily grace solutions and models of submonthly ocean bottom pressure variability. *Journal of Geophysical Research*. doi: 10.1029/2020jc017031

Schmeer, M., Schmidt, M., Bosch, W., & Seitz, F. (2012). Separation of mass signals within grace monthly gravity field models by means of empirical orthogonal functions. *Journal of Geodynamics*. doi: 10.1016/j.jog.2012.03.001

Schmied, H. M., Cáceres, D., Eisner, S., Flörke, M., Niemann, C., Peiris, T. A., ... Döll, P. (2020, March). *The global freshwater availability and water use model WaterGAP 2.2d* (Tech. Rep. No. EGU2020-11434). Copernicus Meetings. Retrieved 2022-07-27, from https://meetingorganizer.copernicus.org/EGU2020/EGU2020-11434.html (Conference Name: EGU2020) doi: 10.5194/egusphere-egu2020-11434

Schneider, U., Becker, A., Finger, P., Meyer-Christoffer, A., Rudolf, B., & Ziese, M. (2016). Gpcc full data reanalysis version 7.0: Monthly land-surface precipitation from rain gauges built on gts based and historic data. *null*. doi: 10.5065/d6000072

Sośnica, K., Jäggi, A., Meyer, U., Thaller, D., Beutler, G., Arnold, D., & Dach, R. (2015, October). Time variable Earth's gravity field from SLR satellites. *Journal of Geodesy*, *89*(10), 945–960. Retrieved 2021-01-25, from https://doi.org/10.1007/s00190-015-0825-1 doi: 10.1007/s00190-015-0825-1

Swenson, S., & Wahr, J. (2002). Methods for inferring regional surface-mass anomalies from gravity recovery and climate experiment (grace) measurements of time-variable gravity. *Journal of Geophysical Research*. doi: 10.1029/

2001jb000576

Tapley, B. D., Bettadpur, S., Ries, J. C., Thompson, P. F., & Watkins, M. M. (2004, July). GRACE Measurements of Mass Variability in the Earth System. *Science*, *305*(5683), 503–505. Retrieved 2022-07-21, from `https://www.science.org/doi/full/10.1126/science.1099192` (Publisher: American Association for the Advancement of Science) doi: 10.1126/science.1099192

Tapley, B. D., Watkins, M. M., Flechtner, F., Reigber, C., Bettadpur, S., Rodell, M., ... Velicogna, I. (2019, May). Contributions of GRACE to understanding climate change. *Nature Climate Change*, *9*(5), 358–369. Retrieved 2022-05-03, from `https://www.nature.com/articles/s41558-019-0456-2` (Number: 5 Publisher: Nature Publishing Group) doi: 10.1038/s41558-019-0456-2

Velicogna, I., Mohajerani, Y., A, G., Mouginot, J., Noël, B., Sutterley, T. C., ... van Wessem, J. M. (2020). Continuity of ice sheet mass loss in greenland and antarctica from the grace and grace follow-on missions. *Geophysical Research Letters*. doi: 10.1029/2020gl087291

Wahr, J., Molenaar, M., & Bryan, F. (1998). Time variability of the Earth's gravity field: Hydrological and oceanic effects and their possible detection using GRACE. *Journal of Geophysical Research: Solid Earth*, *103*(B12), 30205–30229. Retrieved 2020-11-06, from `https://agupubs.onlinelibrary.wiley.com/doi/abs/10.1029/98JB02844` (Formules EWH, conversion bizarre Cnm, Snm en N hauteur geoide) doi: 10.1029/98JB02844

Wang, F., Shen, Y., Chen, Q., & Sun, Y. (2021). Reduced misclosure of global sea-level budget with updated tongji-grace2018 solution. *Scientific Reports*. doi: 10.1038/s41598-021-96880-w

Whitehouse, P. L., Bentley, M. J., Milne, G. A., King, M. A., & Thomas, I. D. (2012). A new glacial isostatic adjustment model for antarctica: calibrated and tested using observations of relative sea-level change and present-day uplift rates. *Geophysical Journal International*. doi: 10.1111/j.1365-246x.2012.05557.x

Śliwińska, J., Nastula, J., & Wińska, M. (2021). Evaluation of hydrological and cryospheric angular momentum estimates based on GRACE, GRACE-FO and SLR data for their contributions to polar motion excitation. *Earth, Planets and Space*. doi: 10.1186/s40623-021-01393-5

Figure 1.

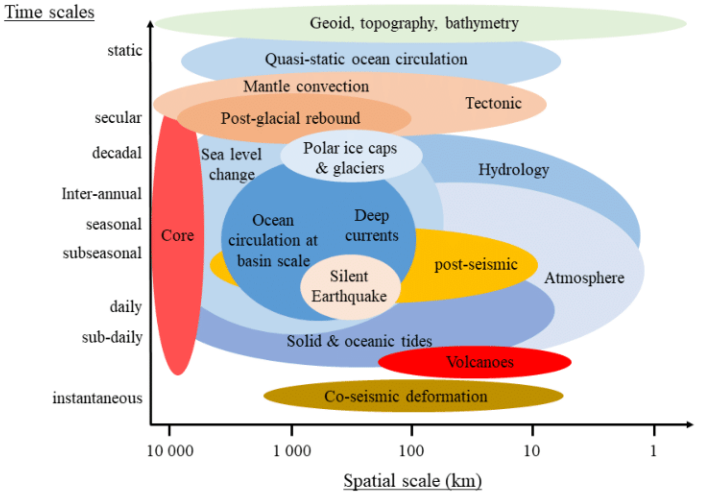
Time scales
static
secular
decadal
Inter-annual
seasonal
subseasonal
daily
sub-daily
instantaneous
Geoid, topography, bathymetry
Quasi-static ocean circulation
Mantle convection
Tectonic
Post-glacial rebound
Sea level change
Polar ice caps & glaciers
Hydrology
Core
Ocean circulation at basin scale
Deep currents
post-seismic
Atmosphere
Silent Earthquake
Solid & oceanic tides
Volcanoes
Co-seismic deformation
10 000
1 000
100
10
1
Spatial scale (km)

Figure 2.

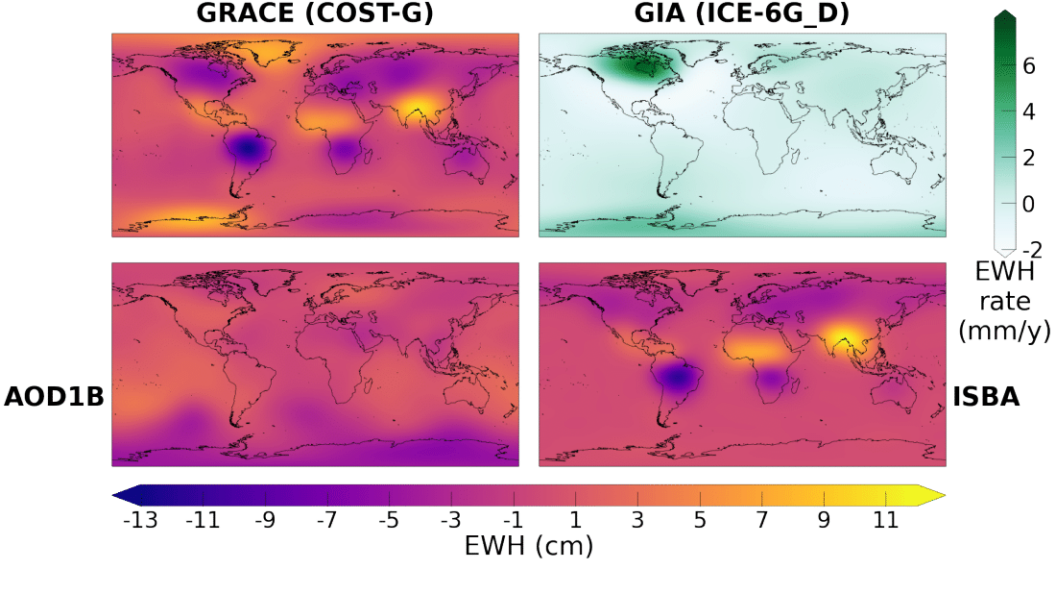
GRACE (COST-G)
GIA (ICE-6G_D)
6
4
2
0
-2
EWH rate (mm/y)
AOD1B
ISBA
-13 -11 -9 -7 -5 -3 -1 1 3 5 7 9 11
EWH (cm)

Figure 3.

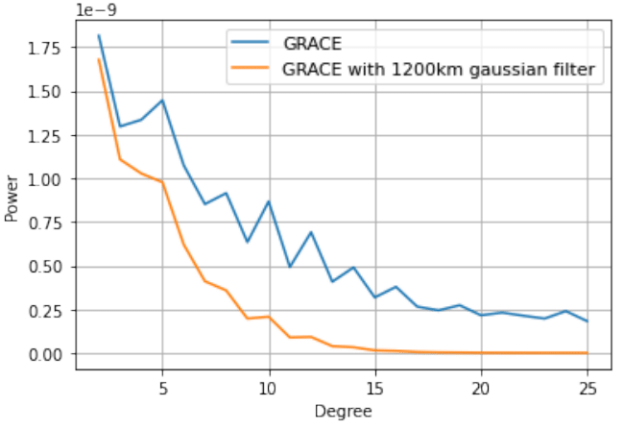
1e−9
1.75
1.50
1.25
1.00
0.75
0.50
0.25
0.00
Power
5
10
15
20
25
Degree
GRACE
GRACE with 1200km gaussian filter

Figure 4.

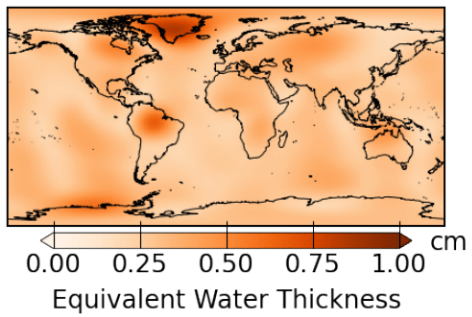

(a) Average of RMS differences in cm EWH spatially represented

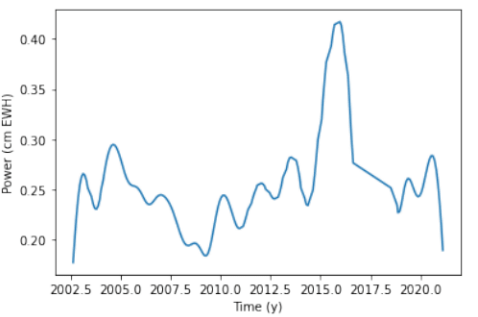

(b) Average of RMS differences in cm EWH represented trough time

Figure 5.

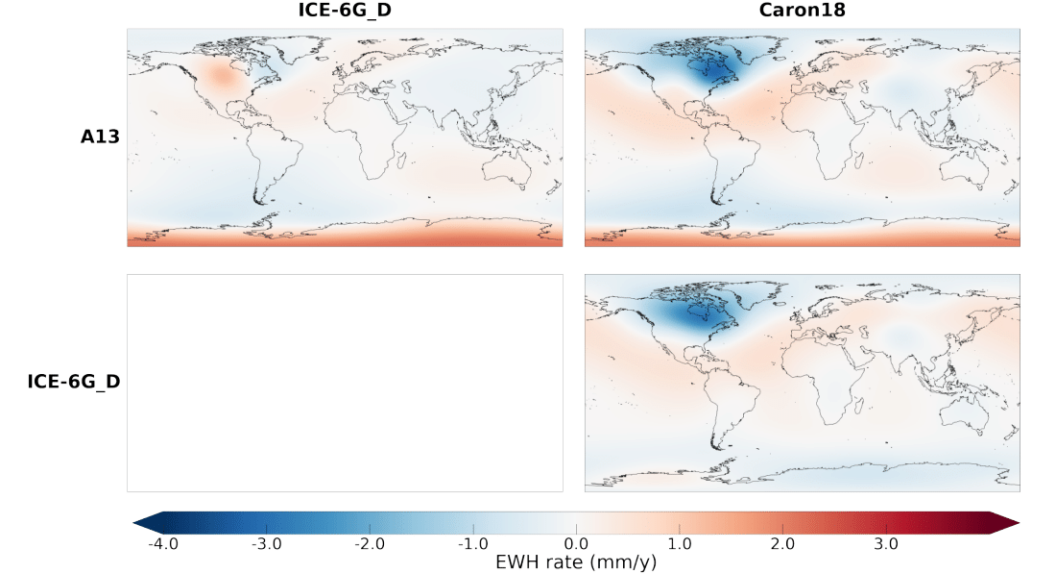
ICE-6G_D
Caron18
A13
ICE-6G_D
-4.0
-3.0
-2.0
-1.0
0.0
1.0
2.0
3.0
EWH rate (mm/y)

Figure 6.

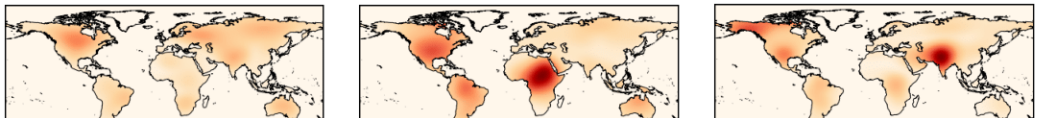

(a) ERA5 minus GLDAS

(b) ISBA minus LSDM

(c) ISBA minus WGHM

Figure 7.

(a) OMCT

(b) MPIOM

(c) T-UGOm

Figure 8.

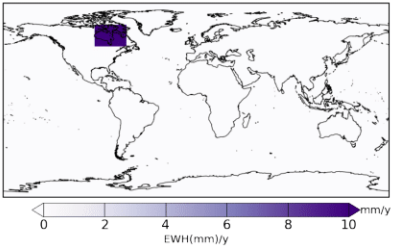

(a) Synthetic signal in North America in EWH

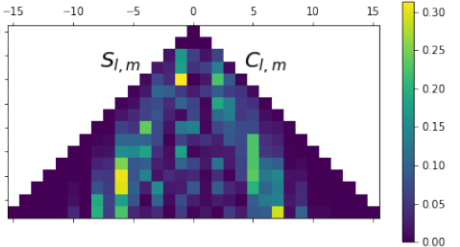

(b) SH power normalized by GRACE standard deviation up to degree 15

Figure 9.

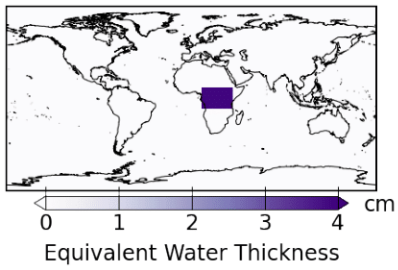

(a) Synthetic 3-yr signal over Africa with an amplitude of 4 cm EWH

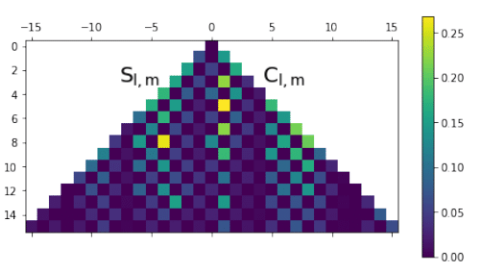

(b) SH power normalized by GRACE standard deviation up to degree 15

Figure A1.

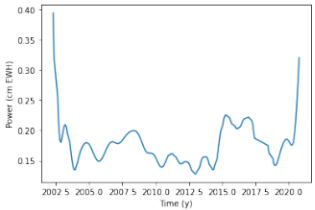

(a) Temporal RMS difference between CSR and JPL solutions

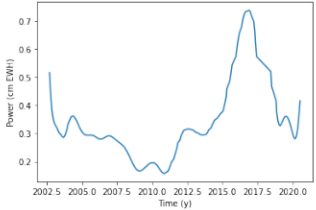

(b) Temporal RMS difference between CSR and GFZ solutions

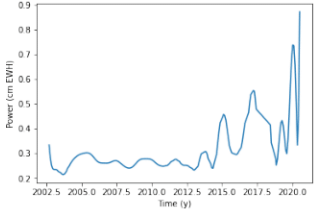

(c) Temporal RMS difference between CSR and GRAZ solutions

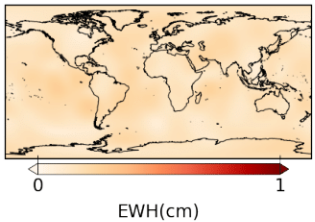

(d) Spatial RMS difference between CSR and JPL solutions

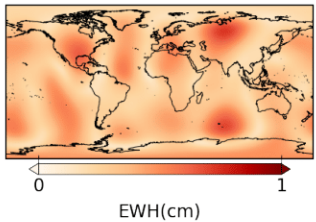

(e) Spatial RMS difference between CSR and GFZ solutions

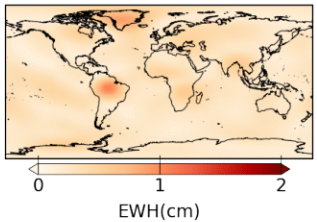

(f) Spatial RMS difference between CSR and GRAZ solutions

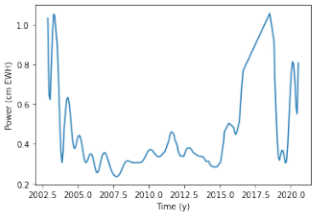

(g) Temporal RMS difference between CSR and CNES solutions

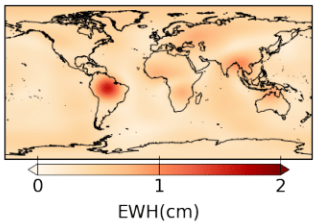

(h) Spatial RMS difference between CSR and CNES solutions

Figure B1.

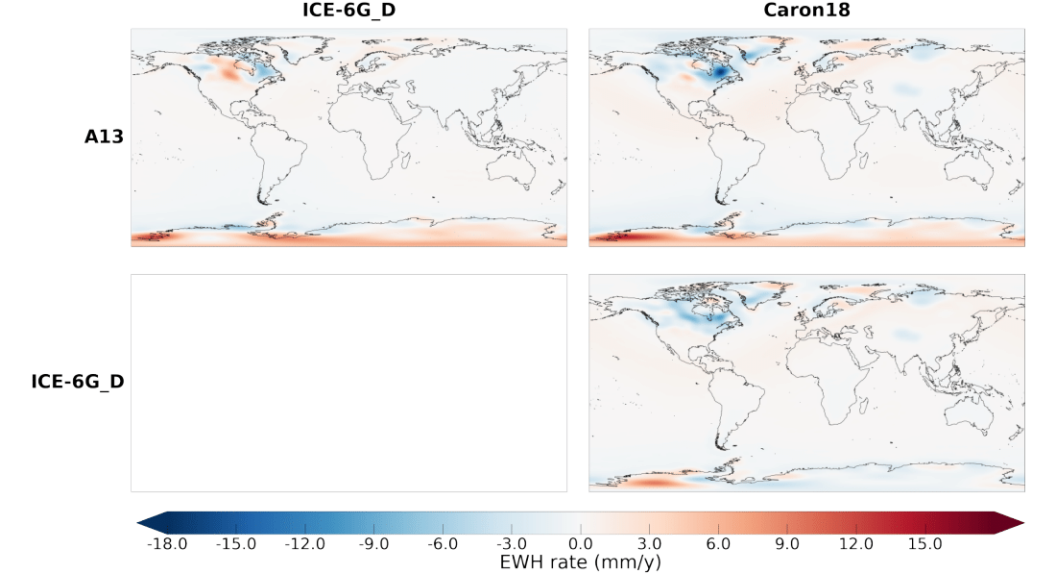
ICE-6G_D
Caron18
A13
ICE-6G_D
-18.0
-15.0
-12.0
-9.0
-6.0
-3.0
0.0
3.0
6.0
9.0
12.0
15.0
EWH rate (mm/y)

Figure E1.

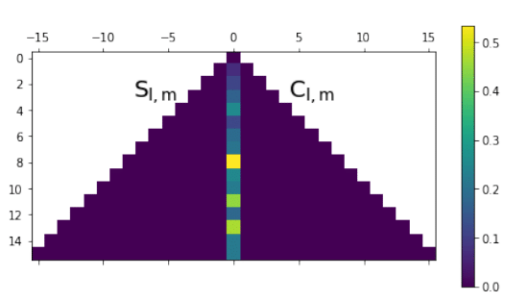

(a) Case $n^o 2$ with synthetic signal under -80^o of latitude

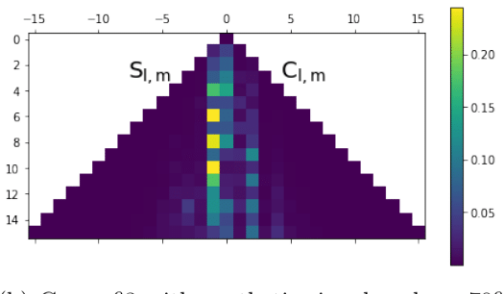

(b) Case $n^o 3$ with synthetic signal under -70^o of latitude and between -160^o and -30^o of longitude

Figure F1.

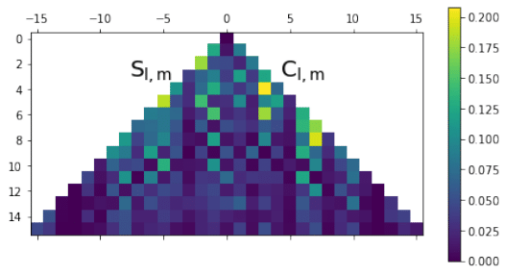

(a) Case $n^o 2$ with synthetic signal over Amazon forest

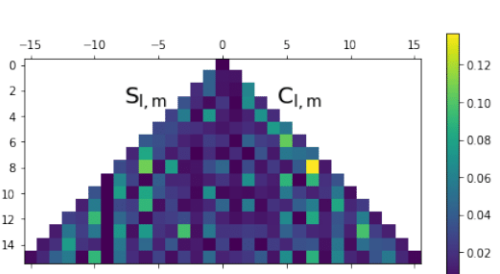

(b) Case $n^o 3$ with synthetic signal over India